Lossada Ana, C. (Orcid ID: 0000-0003-0624-6151)

Hoke Gregory, D (Orcid ID: 0000-0002-3720-3245)

Giambiagi Laura (Orcid ID: 0000-0001-6286-7206)

Mescua José (Orcid ID: 0000-0001-8270-0112)

Suriano Julieta (Orcid ID: 0000-0002-3196-6399)

Detrital thermochronology reveals major middle Miocene exhumation of the eastern flank of the Andes that predates the Pampean flat-slab (33º-33.5ºS)

A. C. Lossada[1], G. D. Hoke[2], L. B. Giambiagi[3], P. G. Fitzgerald[2], J. F. Mescua[3], J. Suriano[3] and A. Aguilar[3]

1: Instituto de Estudios Andinos (IDEAN), Universidad de Buenos Aires, CONICET, Buenos Aires, Argentina.
2: Department of Earth Sciences, Syracuse University, Syracuse, NY, USA
3: IANIGLA, CCT Mendoza, CONICET, Mendoza, Argentina

Corresponding author: Ana C. Lossada (ana.c.lossada@gmail.com)

Key Points:

- Modern river sand thermochronometry constrain timing of exhumation of the Andes in the flat to normal subduction transition
- Main exhumation of Frontal Cordillera in this region occurred at 15.3-17 Ma, prior to the onset of flat-slab conditions
- Timing of exhumation is consistent with an eastward progression of deformation

This article has been accepted for publication and undergone full peer review but has not been through the copyediting, typesetting, pagination and proofreading process which may lead to differences between this version and the Version of Record. Please cite this article as doi: 10.1029/2019TC005764

Abstract

The Cordón del Plata and Cordón del Portillo (32.6º-33.8ºS) are the portions of the Frontal Cordillera that straddle the transition zone between the Pampean flat-slab subduction segment to the north and the normal subduction segment to the south. A complete understanding of how the Frontal Cordillera developed is necessary in order to evaluate different tectonic models for the Andes along with their relation to subduction dynamics and contractional upper-crustal deformation. Detrital apatite fission track thermochronology of modern river sediments that drain the eastern and western slopes of the Cordón del Plata and the northern Cordón del Portillo provide constraints on regional exhumation histories. AFT data from each catchment typically contain multiple age peaks, but all have a prominent 15.3-17 Ma age peak. One catchment, the Las Tunas River has a unimodal distribution at 17.0 ± 1.1 Ma, with a confined track length distribution indicative of rapid cooling at that time. These results, combined with provenance analysis in the adjacent Cacheuta Basin, indicate significant early to middle Miocene (~16Ma) exhumation in the Cordón del Plata and the northern sector of the Cordón del Portillo. Exhumation related to rock uplift occurred prior to the ~11 Ma onset of a flat slab geometry at these latitudes, but immediately after the main east-vergent contractional event in the adjacent Principal Cordillera. Such Frontal Cordillera exhumation fits in an eastward, youngest to the foreland sequence of deformation of the different morphostructural Andean units at ~33º-34ºS, arguing against the recently proposed west-vergent orogenic system at these latitudes.

1 Introduction

The Andes represent the largest non-collisional orogen in the world, a result of a long-lived active oceanic-continent subduction, since at least the Jurassic (Mpodozis and Ramos, 1989; Oliveros et al., 2007). Despite long-term convergence, the topographic growth of the Southern Central Andes (~28º-36ºS) largely occurred during the Miocene, in association with

rapid absolute trenchward motion of South America and an episode of flat subduction (Pardo-Casas and Molnar, 1987; Mpodozis and Ramos, 1989; Ramos et al., 1996; Somoza, 1998; Charrier et al., 2007; Horton, 2018). Today the margin of the Central Andes is characterized by a relatively shallow subduction angle (Isacks and Barazangi, 1976) and two prominent zones of "flat" subduction; the Peruvian (5º-14ºS) and the Pampean (27º-33.5ºS) flat-slab segments (Barazangi and Isacks, 1976; Cahill and Isacks, 1992). Many studies invoke past episodes of flattening of the slab on the basis of geochemistry of igneous rocks or spatial patterns of deformation and magmatism (e.g. Kay and Mpodozis, 2002; Isacks, 1988), such that it is often viewed as a principal element of Andean orogenic development. However, recent work in the Pampean flat-slab points toward major range growth that predates shallowing of the subduction zone (Riesner et al., 2019; Buelow et al., 2018; Suriano et al., 2017; Lossada et al., 2017; Hoke et al., 2015). Moreover, Horton (2018) concludes that changes in plate velocities at the convergent boundary exert a first order control on the tectonic regime governing the construction of the Andes, while flat-slab episodes represent a second order driving process.

Between ~33°-34°S, the Andes span the transition between the Pampean flat-slab and the southern normal-dipping subduction segments (Fig. 1a). Six tectonic provinces subdivide the mountain chain, from west to east: the Coastal Range, Principal Cordillera, Central Depression, Frontal Cordillera, Precordillera, and Pampean Ranges. Two N-S ranges comprise the bulk of the Frontal Cordillera between 32.65°S and 33.8°S: the Cordón del Plata and the Cordón del Portillo (Fig. 1b). These ranges consist of uplifted pre-Jurassic igneous-metamorphic basement blocks, poorly explored due to their high mean elevation and local relief in excess of 4 km.

Despite the preponderance of data indicating a largely east-directed orogen (Ramos et al., 1996; Giambiagi and Ramos, 2002; Giambiagi et al., 2003, 2012, 2015; Farías et al., 2010), a

west-vergent tectonic model was recently proposed for a narrow segment of the Andes between ~33°-34°S. This west-vergent model calls for the uplift and exhumation of the Frontal Cordillera as part of a large west-vergent anticline structure, associated with a blind megathrust located below Principal Cordillera (Armijo et al., 2010; Riesner et al., 2018, 2019). However, there are no clear chronologic constraints for the onset of deformation of the ranges comprising the eastern flank of the Andes that would definitively support this model.

In this paper, we apply AFT thermochronology to modern sediment samples collected from rivers draining the Frontal Cordillera. Our objective is to constrain the timing of exhumation, and by inference rock uplift, along the eastern flank of the Andes between 33º and 34ºS. Detrital fission-track thermochronology uses the single grain ages from multiple detrital grains to quantify the thermal evolution of the catchment area upstream of the sampling point, and to potentially identify and characterize the source region (e.g., Baldwin et al., 1986; Cerveny et al., 1988; Brandon et al., 1998; Garver et al., 1999; Bernet et al., 2001; Willett et al., 2003; Ruiz et al., 2004; van der Beek et al., 2006). By integrating our results with existing thermochronology data, regional structural features, provenance and other sedimentological evidence from syntectonic basins, we evaluate the influence of flat *versus* normal subduction geometry, and at this key latitude, the merits of the west-vergent *versus* east-vergent tectonic evolution paradigms.

2 Tectonic Setting

In the Pampean flat-slab segment (27°-33.5°S, Fig. 1a, 1b, Cahill and Isacks, 1992; Güstcher et al., 2000), the Andes are characterized by high mean elevations in the Principal and Frontal Cordilleras, a lack of active arc-related magmatism, and a large orogenic width with basement-involved deformation resulting in the Pampean Ranges rising through the foreland (Jordan et al., 1983). The origin of the Pampean flat-slab is often linked to subduction of the

buoyant Juan Fernández aseismic ridge below the continental margin (Barazangi and Isacks, 1976; Jordan et al., 1983; Yáñez et al., 2002). Ocean plate reconstructions indicate rapid southward migration of the collision point with the buoyant ridge along 1,400 km of the margin from 20 to 11 Ma (Yáñez et al., 2001), which then becomes fixed at ~33°S. The purported southward sweep of the flat-slab along with the ridge led to the hypothesis of a diachronous north to south onset of contraction along the Frontal and Pre- Cordilleras since ca. 18 Ma (Pilger, 1984; Yáñez et al., 2002; Ramos et al., 2002). Nonetheless, several evidence indicates that the onset of Neogene deformation of the Precordillera was synchronous along its N-S strike (Walcek and Hoke, 2012; Levina et al., 2014; Suriano et al., 2017; Buelow et al., 2018).

The classic model of Andean evolution (Ramos et al., 2002) advocates the sequential, foreland-ward (eastward) advancement of the deformation front during the Neogene, following the shift in arc-related magmatic activity (Kay et al., 1987). This model results in the progressive development of the Principal Cordillera (early to late Miocene), the Frontal Cordillera (late Miocene), the Precordillera (Pliocene) and the Pampean Ranges (Pliocene). According to this interpretation, uplift of Frontal Cordillera and Precordillera, and ultimately the Pampean Ranges across the broken foreland basin, occurred in response to the flattening of the slab since ca. 9 Ma at the representative latitude of 33ºS (Ramos et al., 2002; Giambiagi et al., 2003, Ramos and Folguera, 2009). However, recent work suggests that the Cordón del Plata likely uplifted earlier than previously recognized (Hoke et al., 2015; Buelow et al., 2018, Riesner et al., 2019).

In the normal subduction segment south of 33°S (Fig. 1a), the Andes are characterized by an active magmatic arc straddling the main continental divide, and the mountain chain narrows as the Precordillera and the Pampean Ranges are replaced by growing structures in the Neogene foreland basin sediments, a result of thick-skinned tectonics. Between the flat and

normal subduction segments there is a transition zone (~33°-33.5°S) where the subducted slab has a smooth, yet abrupt bend to a normal subduction geometry (Cahill and Isacks, 1992; Yáñez et al., 2001; Gans et al. 2011; Anderson et al., 2007). The Cordón del Plata and Cordón del Portillo ranges are the portions of the Frontal Cordillera that occupy the transition in subduction geometry (Fig. 1b, 1c and 1d, Fig. 2).

The Cordón del Plata is a NNE-trending, 4,000 m high ridge composed of Proterozoic to Devonian medium- to high-grade metamorphic rocks, late Carboniferous to early Permian siliciclastic deep marine sedimentary rocks and felsic intrusive rocks that are overlain by the thick (2-4 km) Permian to Triassic Choiyoi Group felsic igneous succession that dominates the range (Fig. 2, Polanski, 1957; Caminos, 1965; Heredia et al., 2012). Pre-Andean deformation of Paleozoic rocks that comprise part of the Frontal Cordillera at the study latitudes occurred during the Late Devonian to early Carboniferous (Chanic orogeny, Polanski, 1957) and late Carboniferous to Early Permian (San Rafael orogeny, Ramos, 1988, Kleiman and Japas, 2009). Many of the N-S to NNE-striking, east-vergent, contractional Pre-Andean structures were reactivated during the Andean orogeny, and control the morphology of the range (Giambiagi et al., 2014). The La Carrera fault system is located at the eastern boundary of the Cordón del Plata (Fig. 1c, Fig. 2) and was responsible for its Cenozoic uplift (Caminos, 1964, 1965; Polanski, 1972; Cortés, 1993; Folguera et al., 2004; Casa, 2005). It comprises four NNE-striking, east-vergent, reverse faults. Although major activity on this fault system occurred during the Miocene (Caminos, 1964; Polanski, 1972), neotectonic activity is well documented (Fauqué et al., 2000; Folguera et al., 2004; Casa et al., 2010).

The Cordón del Portillo is composed of a Proterozoic metamorphic basement and a Paleozoic sedimentary cover intruded by Permo-Triassic Choiyoi granitoids (Fig. 2, Polanski, 1964, 1972). It is bounded to the east by deep-seated, east-vergent faults, which juxtapose pre-

Jurassic basement rocks over the middle Miocene to Quaternary sedimentary rocks deposited in the foreland basin (Polanski, 1964; Giambiagi et al., 2003). Its western sector corresponds to a gently west-dipping paleosurface constituted by Choiyoi Permo-Triassic volcanic rocks and Carboniferous black shales, on top of which late Cretaceous limestones unconformably rest (Tunik, 2003). The northern region of the Cordón del Portillo was affected by NNE-striking faults –essentially the southern prolongation of the La Carrera fault system– whereas in the south, the N to NNW striking structures are grouped into the Portillo fault system (Fig. 2) (Polanski, 1957; Kozlowski et al., 1993; Giambiagi et al., 2003).

The exhumation history, and by inference the rock uplift history, of the different morphotectonic units at 33°-33.5ºS (Fig. 1b) is recorded in the >2.2 km Cenozoic synorogenic sedimentary rocks that fill the Cacheuta foreland basin immediately adjacent to the La Carrera fault system (Ramos, 1988; Irigoyen et al., 2000)(Fig. 1b, Fig. 2) and in the ~1.9 km thick sedimentary succession of the Alto Tunuyán basin located between the Frontal and Principal cordilleras (Giambiagi, 1999, 2000; Ramos et al., 2000; Giambiagi et al., 2003)(Fig. 1b, Fig. 2). Recent provenance studies in these basins (Buelow et al., 2018; Porras et al., 2016) suggest that the Frontal Cordillera rose prior to ~9 Ma, earlier than previously proposed by Giambiagi et al. (1999, 2001, 2003), Irigoyen et al. (2000) and Ramos et al. (2002).

In addition to uncertainties regarding the timing of deformation of the Frontal Cordillera, debate persists regarding the vergence direction of the fold-thrust belt at this latitude (Fig. 3). The vast majority of tectonic models for the Andes between 32° and 34°S conclude an eastward advance of deformation (Fig. 3A), based on an extensive array of evidence for the timing of uplift and exhumation of the different morphostructural units (Farías et al., 2008; Fosdick et al., 2015; Pinto et al., 2018), present-day GPS vectors (Brooks et al., 2003), east vergence of the main structures of the Frontal Cordillera (Polanski, 1972; Cristallini and

Ramos, 2000) uplifting Proterozoic (Polanski, 1972) and lower Paleozoic rocks (Heredia et al., 2012; Giambiagi et al., 2014), and the record of orogenic growth in foreland basins (Ramos et al., 1996; Levina et al., 2014; Buelow et al., 2018, and reference therein). In contrast, the relatively recently proposed conceptual west-vergent tectonic model for the Andes at the latitude of ~33.5°S (Armijo et al., 2010; Riesner et al., 2017, 2018, 2019) (Fig. 3B) involves an east-dipping crustal-scale detachment beneath Frontal Cordillera, named the West Andean Thrust (WAT), that shallows to the west until it reaches the surface along the western flank of the Andes. In the WAT model, deformation initiated simultaneously in the Frontal Cordillera and along west-vergent thrusts located in the western flank at ~20-25 Ma, and propagated westward. According to this model, the Aconcagua fold-and-thrust belt uplifted passively as a secondary back-thrust structure since ~20-25 Ma to present. It is noteworthy that Farías et al. (2010), using nearly identical data, interpreted the deep crustal structure as a major east verging ramp-detachment structure, in support of the traditional eastward-vergent tectonic model for the Andes.

2.1 Provenance signal from syntectonic basins

2.1.1 The Cacheuta Basin

The > 2,200 m thick Neogene strata of the Cacheuta Basin (Fig. 2) record a detailed history of Andean orogenic exhumation at 33º to 33.5ºS that spans ~12 Myr (ca. 20 Ma to younger than 7.5 Ma), based on zircon U-Pb geochronology (detrital and tuff samples) (Buelow et al., 2018). Five Neogene formations are present in the basin, from oldest to youngest: Mariño, La Pilona, Tobas Angostura, Río de los Pozos, and Mogotes (Fig. 2) (Yrigoyen, 1993; Irigoyen et al., 2000), that reflect the sediment flux produced during episodic eastward thrust belt propagation. The Mariño Formation consists of ~1,000 m of intercalated pebble conglomerate, lithic arenite, siltstone and mudstone that unconformably overlies the

Paleogene Divisadero Largo Formation. The La Pilona Formation is ~900 m thick and consists of intercalated pebble to cobble conglomerate, lithic arenite and subordinate fine-grained clastic strata. The Tobas Angostura Formation consists of ~150 m of recessive, intercalated volcanic tuff and reworked pyroclastic debris, reflecting a pulse of late Miocene volcanism (constrained by zircon U-Pb dating from ca. 8.3 at the base to ca. 7.4 Ma next to the upper contact, Buelow et al., 2018). The Río de los Pozos Formation is composed of distinctly yellow, poorly consolidated lithic arenite, sandy conglomerate, and multicolored fine-grained clastic sediments. Finally, the youngest stratigraphic unit, the Mogotes Formation, consists of disorganized pebble to boulder conglomerate separated by mudstones and siltstones.

Detrital zircon U-Pb geochronology, conglomerate clast counts, thin section petrography, and sedimentologic analyses from Buelow et al. (2018) record progressive orogenic exhumation of the Principal Cordillera, Frontal Cordillera, and Precordillera during early to middle Miocene time. They found that conglomerates throughout the basin are dominated by rhyolite clasts, and a distinctive Permo-Triassic detrital zircon signature is present even in the lower levels of the Mariño Formation (~20-19 Ma depositional age). The Permo-Triassic detrital zircon signal is pervasive, also comprising a major component of the detrital zircon age spectra in the Paleogene Divisadero Largo Formation (Mahoney et al., 2016; Mescua et al., 2017, Fig. 2), and the Jurassic to Cretaceous Neuquén Basin succession (Naipauer et al., 2015; Horton and Fuentes, 2016). Although the upper Paleozoic to lower Mesozoic magmatism of the Choiyoi Group is present predominantly in the Frontal Cordillera ranges (Fig. 2), the Permo-Triassic zircons in the lower levels of Mariño Formation (~20 Ma) could represent recycled material from the underlying Divisadero Largo Formation and/or the Mesozoic sequences from the northern extend of the Neuquén Basin in the Principal Cordillera. In contrast, a marked influx of Choiyoi Group clasts, together with an increase in

Permo-Triassic and Mesoproterozoic zircons, likely from the Choiyoi Group and Paleozoic strata of the Cordón del Plata, and the change to a more energetic depositional environment is observed within the Mariño Formation at 16.3 ± 0.83 Ma (U-Pb detrital zircon) (Buelow et al. 2018). The later suggesst an uplift pulse of Frontal Cordillera around 16 Ma.

2.1.2 The Alto Tunuyán Basin

The syntectonic Alto Tunuyán Basin (33.67°S, Fig. 2) developed on the eastern side of the southern Aconcagua fold-and-thrust belt that forms the Principal Cordillera, and records the timing of thrusting (between ~15 to 6 Ma) within this structural unit as well as the onset of deformation of Cordón del Portillo to the east (Giambiagi, 2000; Giambiagi et al., 2003; Porras et al., 2016). The Alto Tunuyán basin infill (~ 1,900 m) is divided into three formations, from oldest to youngest: the Tunuyán Conglomerate, the Palomares and the Butaló (Fig. 2). The oldest unit, the Tunuyán Conglomerate, consists of up to 1,400 m of conglomerates and sandstones deposited in an alluvial-fan setting. The Palomares Formation consists of 200 m of volcaniclastic and clastic sediments also deposited in an alluvial-fan setting. At the top of the sequence, the Butaló Formation consists of fluvial and lacustrine deposits of more than 300 m that records the final infilling of the intermontane basin between the Frontal and Principal Cordilleras. Based on clast-counts in conglomerates and paleocurrent analyses, Giambiagi et al. (2003) proposed a basin evolution in which the Tunuyán Conglomerate (15 to 9 Ma) records deformation and unroofing of the Aconcagua fold-and-thrust belt in the Principal Cordillera, whereas the Palomares Formation is related to exhumation of the Cordón del Portillo in the Frontal Cordillera between 9 to 6 Ma. While Porras et al. (2016) document the presence of Permo-Triassic (Choiyoi) and Proterozoic contributions in the detrital zircons of sandstones within the Tunuyán Conglomerate, it is equivocal as to whether or not it points towards erosional influx from the Frontal Cordillera

or it could represent recycled material from the Mesozoic sedimentary rocks in the Principal Cordillera (Tunik et al., 2012).

3 Methods

Low-temperature thermochronology constrains the timing and rate of cooling of rocks as they are exhumed toward the surface of the earth. Different minerals and methods are sensitive over a variety of temperature ranges, and therefore have the potential of constraining diverse tectonic processes at different crustal levels (e.g., Gallagher et al., 1998; Malusà and Fitzgerald, 2019a). Fission track (FT) thermochronology is based on the retention of radiation damage (fission tracks) formed during the spontaneous fission of ^{238}U in uranium-bearing minerals (commonly apatite or zircon). The closure temperature for AFT is on the order of 110ºC (±10ºC) depending on composition and cooling rate (e.g., Gleadow and Duddy, 1981; Gleadow et al., 1989; Green et al., 1989). The partial annealing zone (PAZ) for the AFT system is ~110-60°C (Gleadow and Fitzgerald, 1987). Determining the concentration of ^{238}U and density of spontaneous fission tracks yields FT ages that, together with the kinetic parameter of confined track lengths, may provide robust constraints on the thermal history of rocks as they traverse the upper 4-5 km of the crust, assuming typical geothermal gradients. Confined track lengths are not typically measured on detrital samples because individual detrital grains cannot be assumed to represent the sample thermal history if there are multiple single grain age peaks. However, where there is only one age peak in a sample, it is possible to define, by determining the confined track length distribution for that sample, whether that sample is comprised of grains that have all rapidly cooled and therefore whether that age-peak represents a simple rapid cooling/exhumation event.

A common approach to understanding either the provenance of sediments or the exhumation history of the source region is the analysis of modern sediments or sedimentary rocks using one or more thermochronologic techniques (e.g., Baldwin et al., 1986; Cerveny et al., 1988; Brandon and Vance, 1992; Brandon et al., 1998; Garver et al., 1999; Bernet et al., 2001; White et al., 2002; Willett et al., 2003; van der Beek et al., 2006; Bernet, 2019). As an indirect sampling strategy, the detrital thermochronology approach has some advantages over a direct bedrock sampling strategy: (i) as multiple geologic units are potentially represented in one detrital sample, the record of exhumation preserved in sediments may be much longer than that from exposed bedrock within the orogen, (ii) a single river sample should provide a suite of apatites or zircons that are representative of catchment hypsometry, although this is dependent on the fertility of different lithologies and the uniformity of denudation rates throughout the basin (e.g., Ruhl and Hodges, 2005; Garver et al., 1999). Modern river sediment thermochronology is particularly useful in areas of steep relief and low accessibility, as it allows a reconstruction of the grain-age distribution of the sampled catchment (e.g., Garver et al., 1999; Brewer et al., 2003; Ruhl and Hodges, 2005, Gallagher and Parra, 2020). Under the ideal conditions of uniform mineral fertility and erodibility, the thermochronometric ages yielded from an individual sample represent the cooling age-elevation distribution within the catchment, with grains having older apparent ages typically eroded from high elevations, relative to grains with younger apparent ages eroded from lower levels (e.g., Bernet et al., 2004; Resentini and Malusà, 2012). Even in the absence of ideal conditions, the grain-age distributions of modern river samples provide an estimation of the erosional pattern over a large area within the adjacent orogen. The Malusà et al. (2016) quantitative approach for mineral fertility determinations shows that apatite and zircon fertility values may range over three orders of magnitude from one lithology to another, and

that metamorphic and plutonic rocks generally have higher apatite and zircon concentrations than sedimentary rocks.

Double-dating approaches that pair, for example, zircon (U-Th)/He ages with U-Pb ages (e.g., Reiners, 2005) can be undertaken on the same detrital grains in order to confirm that the thermochronometer ages are indeed due to exhumation related cooling. If ages are the same, then grains are typically assumed to be volcanic in origin, otherwise the lower-temperature cooling ages are interpreted in the context of exhumation. We did not undertake double dating in this study because all AFT ages are younger than crystallization or sedimentary ages within each catchment (see Figure 2). Moreover, thermal reheating is unlikely because there are no Cenozoic volcanic units within the sampled catchments. Thus, all AFT ages are interpreted to reflect cooling associated with exhumation.

For sedimentary rocks that have not been thermally altered (i.e. non-reset), the lag-time (e.g., Cerveny et al., 1998; Brandon and Vance, 1992; Garver et al., 1999; Ruiz et al., 2004; Malusa and Fitzgerald, 2020) represents the time difference between the apparent age (assumed to represent a closure temperature age) from a rock sourced in a mountainous source region and the depositional age. Because the timescale from erosion to deposition is regarded as geologically negligible relative to that of exhumation (Brandon and Vance, 1992), lag-time is the difference between the cooling age and the depositional age (Brandon et al., 1998; Garver et al., 1999). Converting lag-time to an average exhumation rate does require basic assumptions regarding the thermal structure of the upper crust and whether or not the apparent age really represent monotonic cooling through the closure isotherm or a partially annealed/reset age. Also, determining an average exhumation rate assumes that the source rock is cooled/exhumed within one orogenic cycle. For modern river detritus, with a stratigraphic age of “zero”, the youngest age mode can be used to constrain the average exhumation rate of the source area (e.g., Malusà and Fitzgerald, 2019b). For example, a

sample with a polymodal grain-age distribution, can typically be deconvolved into different grain-age subgroups; the defined mode for the youngest age component (t_1) is then assumed as the cooling age (if the area was rapidly exhumed), and the depositional age, t_0, of the sample is zero. Thus, lag-time is calculated as the difference between t_0=0 and t_1. Assumed, or independent, constraints of the paleo-geothermal gradient since the youngest age mode (t_1) allows an estimate of the closure depth (Z_c) and hence calculation of an average exhumation rate (Z_c/t_1). Or, lag-time can be converted into an average one dimensional exhumation rate by using graphs that take into account advection of isotherms due to rapid exhumation (e.g., Fig. 9.5 in Braun et al., 2006).

Four detrital samples from modern river sediments were collected in the Arroyo Grande, Las Tunas, Eastern Río Blanco and Western Río Blanco rivers (samples A13-14, A13-15, A13-16 and A13-17, respectively, Fig. 1b, Fig. 2). The >1,850 km^2 drainage area of these rivers comprises a substantial portion of the Cordón del Plata and the northern Cordón del Portillo ranges (Fig. 2) where local relief is between 3.5 and 5 km. The outcropping rocks upstream of the sampling locations are (i) Ediacaran to lower Paleozoic metamorphic rocks (metapelite, metasandstone, schist and amphibolite), (ii) upper Carboniferous marine sediments intercalated with basaltic lavas and continental sedimentary rocks, (iii) Permo-Triassic felsic igneous rocks of the Choiyoi Group (Fig. 2), and (iv) Cenozoic sedimentary rocks. The lithology-elevation distribution for each catchment is shown in figure 4.

At each sampling locality, ~ 3 kg of sand-sized modern river sediment was collected near the active channel at low-flow conditions (winter). The heavy mineral fraction was concentrated using a Wilfley table and apatite grains were separated using conventional magnetic

separation and heavy liquid techniques. Apatites were prepared for FT analysis using the external detector method (Gleadow, 1981), with a low-U muscovite external detector. Samples were irradiated in the slow soaker position B-3 (thermal column number 5) at the Oregon State University Reactor Facility with a total requested fluence of $1x10^{16}n.cm^{-2}$. Neutron fluence was monitored using the CN5 standard glass. The mounts were counted at a magnification of 1250x on a computerized stage, with a zeta of 362 ± 14 (1σ) obtained for Lossada based on IUGS age standards Durango, Fish Canyon and Mount Dromedary apatites as detailed in Hurford and Green (1982) and Hurford (1990). One hundred grains per sample (when available) were measured to obtain an age distribution. In addition, Dpar values (diameter of etched spontaneous fission tracks etch pits measured parallel to crystallographic c-axis) were measured for each counted grain. We also measured confined track lengths for sample A13-15, the only sample with a unimodal age peak. AFT data is shown in Table S1. We present fission-track grain-age (FTGA) data in radial plots (Galibraith, 1990) and density plots (Fig. 5), obtained with RadialPlotter and DensityPlotter programs (Vermeesch, 2009, 2012), employing both PDP (Probability Density Plot) and KDE (Kernel Density) estimators, with a set bandwidth of 15 Ma. The RadialPlotter software identifies and extracts component ages from mixed age populations. For each sample, FTGA distributions were decomposed into discrete main grain-age components (P_1 to Pn, Fig. 5) employing a mixture modeling algorithm, manually selected after the fission-track data has been log transformed (following Galibraith and Green, 1990). Defined age components and proportion per sample are reported in Table 1, and are indicated in the radial and density plots (Fig. 5).

4 Results

FTGA distributions exhibit large dispersion, with grain ages ranging from 0 to ~467 Ma and a maximum sample dispersion of 102%. Radial plots (Fig. 5) are open jaw-type for most samples in our dataset, meaning that multiple age subpopulations are present and a mixture model needs to be applied. Dpar values for single grains have a large variation, between 0.75 μm and 4.05 μm (Table S1), as expected for detrital samples. Single grain ages and Dpar values show no positive correlation (Fig. 5, Fig. S1), which indicates that the ages are not reflecting kinetic variations. Instead, age variation more likely represents the distribution of bedrock AFT ages within the catchments. Central ages range from 20.8 ± 2.2 Ma (1σ) to 90.6 ± 8.5 Ma, although central ages can be misleading in cases of large dispersion, and where there are multiple age populations. All samples fail the Chi-square test which is to be expected as they are detrital samples with grains sourced from across the catchment. Thus, grains represent a mixture of certain proportions of different age components from high elevation (presumably older ages) and lower elevation (presumably younger ages) sectors of a high-relief catchment. FTGA distributions were decomposed into one to four age peaks (P1 to P4, Table 1). All samples resolve a major lower to middle Miocene peak (P1) between 15.3 ± 1.1 and 17.0 ± 1.1 Ma, which are consistent within uncertainty. The remaining, more poorly constrained age modes include a ca. 57 Ma (P2) observed in sample A13-14, a mid-Cretaceous peak of ca. 85-110 Ma (P3) defined in samples A13-14 and A13-16, and a broad ca. 198-150 Ma Jurassic peak (P4) found in samples A13-14, A13-16 and A13-17 (Table 1). These older population peaks (P2, P3 and P4, Table 1) likely represent partially reset ages, given that they are not well resolved and do not correlate from one sample to another (Fig. 4 and 5). For these reasons we focus on the interpretation of P1 which is clearly resolved by both estimators (KDE and PDP) in all analyzed samples. For sample A13-15, the single grain age distribution shows a unimodal peak with a long tail of older ages. The few older grains are presumably most likely sourced at higher elevations where rocks have resided in a PAZ

prior to rapid cooling at ca. 15.3-17 (±1.1) Ma. The 15.3-17 Ma unimodal peak is interpreted as representing simple rapid cooling. We tested that interpretation by measuring the confined track lengths for sample A13-15 (Table S1, Figure 5). The track length distribution has a long mean length (>14 μm) and low standard deviation (1.3 μm), indicating rapid cooling through the partial annealing zone shortly after 17.0 ± 1.1 Ma (see Figure 5). However, we also note the presence of a few short tracks, likely annealed while the few older (higher elevation) grains were resident in a PAZ, prior to rapid cooling. Based on the consistency of the 15.3-17 (±1.1) Ma peak age in all four samples, we assume that age peak P1 reflects a rapid cooling event for Frontal Cordillera at ~16 Ma. Applying the time-lag approach to P1, by assuming a closure temperature of ~110°C and a paleo-geothermal gradient of ~25°C/km, yields an average exhumation rate of ~275 m/Myr.

5 Discussion

5.1 Interpretation of detrital FTGA signal

Of the four age peaks identified across the catchments, only the early to middle Miocene (P1, 15.3-17 Ma) is persistent across samples and maps unambiguously (Fig. 4) as a single rapid cooling event (based on the track length distribution), which we interpret as due to rock uplift associated with a coherent tectonic episode. To further evaluate this interpretation we explore geologic interpretations in the context of additional evidence from syntectonic basins. We interpret the older population peaks (P2, P3 and P4) as partially reset ages. The Las Tunas catchment, the only catchment that presents a unimodal cooling age signature (Fig. 4), predominantly exposes Proterozoic to lower Paleozoic metamorphic rock and late Paleozoic sedimentary rocks that are deeply exhumed from below the AFT partial annealing zone prior to rapid cooling that initiated at ~15.3-17 Ma. In contrast, the bedrock geology of the Río Blanco West, Río Blanco East and Arroyo Grande catchments, that yielded multimodal single grain age distributions, are characterized by high percentages of Permo-Triassic Choiyoi

Group and/or Triassic granitoids (Fig. 4). Detrital single grain ages from these rocks have multiple peaks because they were eroded from shallower crustal levels that presumably represent rocks located within the partial annealing zone at the time rapid cooling initiated, and therefore exhibit partially reset cooling ages, and/or sample across a paleo-topography with different exhumational levels with a variety of age – paleo-elevation profiles.

5.1.1 Exhumation in the early to middle Miocene

The strong presence of the 15.3-17.0 (±1.1) Ma age mode (P1) across basins (Fig. 5, Table 1) suggests a major, regional cooling event affecting the Frontal Cordillera at that time. The confined track length distribution in the only sample (A13-15, Fig. 5) with a unimodal 17.0 ± 1.1 Ma age peak, demonstrates rapid cooling with little or no residence time within the partial annealing zone. We interpret this rapid cooling episode as the result of erosional exhumation during the early part of the Andean orogeny. The timing of exhumation recorded by P1 is broadly coeval with the increase in sediment sources from the Choiyoi Group in the Cacheuta Basin (Buelow et al., 2018), reinforcing our model of an emerging Frontal Cordillera during early to middle Miocene (ca. 16 Ma). Major exhumation in the Frontal Cordillera indicated by our data is slightly younger than the onset of the main deformation phase in the Aconcagua fold-and-thrust belt, which occurred at 20 Ma (Ramos et al., 2002), and coincident with the migration of the calcalkaline volcanic-arc axis between ~17 and 16 Ma (Carrasquero et al., 2017) from west (Farellones Fm., 23-17 Ma, Charrier et al., 2002; Nyström et al., 2003) to east (Aconcagua Volcanic Complex, 15.8-8 Ma, Ramos et al., 1996) across the Principal Cordillera. The eastward volcanic-arc migration coincides with the end of contractional deformation in the northern Aconcagua fold-and-thrust belt (Cegarra and Ramos, 1996). We do not interpret the single grain age peak P1 (15.3-17 Ma) as associated with thermal resetting triggered by volcanic arc migration because, in that case, the age peak

would be mainly composed of less retentive (low Dpar values) apatites, which is not observed in our data (Fig. 5, Fig. S1).

With respect to the spatial extent of Miocene rapid cooling and exhumation, our data indicate that exhumation of the northern sector of the Cordón del Portillo (sample A13-14, Arroyo Grande, Fig. 5) was synchronous with that of the Cordón del Plata (remaining samples) at ca. 16 Ma. We interpret that this area was rapidly exhumed along the same NNE trending La Carrera fault system and its southward prolongation (Fig. 6b, stage 16-13 Ma). Exhumation of the Frontal Cordillera during the early to middle Miocene demonstrated by our data is contemporaneous with deposition of the Tunuyán Conglomerate, yet it appears that no alluvial fans from the rising Frontal Cordillera extended westward enough to interfinger with those of the simultaneously active Principal Cordillera. Permian to Triassic detrital zircon ages are present in the Tunuyán Conglomerate (Porras et al., 2016); however, given their ubiquity in the Mesozoic sandstones of the Aconcagua fold-and-thrust belt and clear eastward paleoflow (Giambiagi et al 2003), it is difficult to ascribe their source uniquely to the Frontal Cordillera (Fig. 6b, stage 16-13 Ma). Subsequent rock uplift in the Frontal Cordillera resulting in westward migration of alluvial fans into the Alto Tunuyán Basin can be inferred from the appearance of Frontal Cordillera clasts, west directed paleoflow (Giambiagi et al., 2003), and Permian to Triassic zircons (Porras et al. 2016) recorded in the latest Miocene Palomares Formation (9-6 Ma, Fig. 2, Fig. 6c). The 9-6 Ma period of rock uplift of the southern Cordón del Portillo agrees with a ~2-km surface uplift of the Alto Tunuyán basin determined by Hoke et al. (2014) using stable isotope data from pedogenic carbonates from the basin. However, this 9-6 Ma compressive pulse is not captured in our detrital AFT dataset, particularly in Sample A13-14 that corresponds to the Arroyo Grande catchment, carved in the Cordón del Portillo range. Possible explanations for the lack of ~9 Ma AFT cooling ages are (i) the ~9 Ma event is of limited magnitude (less than ~110°C of cooling or

exhumational equivalent) and so any rocks that cooled rapidly at ~9 Ma have yet to be eroded, or (ii) this ~9 Ma rapid cooling event associated with rock uplift and exhumation at that time was not regional in extent. The ~9 Ma event may be restricted only to the southern end of the Cordon del Portillo where exhumation occurred along the NW trending El Portillo fault system, and did not affect (or was a minor reactivation at) the Cordón del Plata range and the northern part of Cordón del Portillo range, uplifted by the same La Carrera fault system (Fig. 2). The second scenario proposed above is supported by geologic evidence from the synorogenic Cacheuta Basin that record a major influx of Frontal Cordillera detritus at 16.3 ± 0.83 Ma, with no evidence for a ~9 Ma reactivation (Buelow et al., 2018). While our data do not excluded the occurrence of a ~9 Ma cooling/exhumation event related to flattening of the slab, integrating geological constraints from the synorogenic Cacheuta basin regarding rock uplift history of these ranges makes the case that the ~9 Ma pulse was not the main exhumation event, at least in the Cordón del Plata range.

Reconciling studies of exhumation (this work), provenance from Alto Tunuyán Basin (Porras et al., 2016; Giambiagi et al., 2003) and paleoaltitude (Hoke et al., 2014) helps to identify different pulses of rock uplift/exhumation of the Cordón del Portillo, and an improved chronology of fault activity. Faulting along the pre-existing La Carrera fault system started to exhume the Cordón del Plata and northern sector of Cordón del Portillo by ca. 16 Ma, which is supported by provenance evidence from Cacheuta Basin (Buelow et al., 2018) and detrital zircons in the Tunuyán Conglomerate (Porras et al., 2016), but it was not until ~9 Ma that coarse grained detritus shed off the growing southern Cordón del Portillo were deposited in the Alto Tunuyán Basin (Fig. 6). From these observations it follows that exhumation of the Cordón del Portillo was segmented through two different fault systems; the La Carrera fault system to the north and the El Portillo fault system to the south.

Our results confirm evidence recently inferred from synorogenic basins (Buelow et al., 2018), that lower to middle Miocene exhumation of the Frontal Cordillera in the transition zone initiated at ca. 16 Ma. This timing for the onset of exhumation is substantially earlier than previously proposed by Giambiagi et al. (2003) and Ramos et al. (2002), who amongst others, tightly linked deformation in the Frontal Cordillera to the development of flat slab conditions at ca. 9 Ma at the study latitude. Moreover, our proposed timing of deformation for the Frontal Cordillera is contemporaneous with the last phase of deformation in the Aconcagua fold-and-thrust belt, during an out-of-sequence thrusting event (Cegarra and Ramos, 1996).

The 15.3-17 Ma AFT P1 age peak is consistent with recently published apatite (U-Th)/He ages from a vertical sampling profile at the Cordón del Portillo (Riesner et al., 2019), that indicates exhumation started prior to ~12-14 Ma. Those authors further suggested Frontal Cordillera exhumation began at ~20 Ma based on zircon (U-Th)/He ages from the same vertical transect and their interpretation of an exhumed ZHe partial retention zone. The youngest single grain age in the lowermost sample is 22.3 ± 0.2 Ma, and was interpreted to mark the onset of rapid cooling, although their ZHe ages exhibit high dispersion up to 116 Ma, likely a result of varying [U]. AHe results from Hoke et al. (2015) in the vicinity of Riesner et al. (2019) sampling area were complex, but the authors interpreted an initiation of slow exhumation for the Cordón del Portillo at 20 to 25 Ma, with a rapid acceleration at ~10 Ma. Following Hoke et al. (2015), Riesner et al. (2019) also concluded that the Frontal Cordillera was a positive topographic feature during the early stages of the Cacheuta Basin sedimentation, because Permo-Triassic zircons and rhyolitic detritus are present. However, derivation of Permo-Triassic zircons and rhyolitic detritus into the Cacheuta Basin was not exclusively from the Frontal Cordillera at that time, as the Principal Cordillera was also a sedimentary source to Cacheuta Basin (Buelow et al., 2018). In addition, Frontal Cordillera detritus that reached the Cacheuta Basin at ~20 Ma are rounded and fine grained, indicating

the source was more likely distal (i.e., from other blocks to the northwest, such as the Cordón del Espinacito region of the Frontal Cordillera, Fig. 6), rather than proximal (i.e., not necessarily from Cordón del Plata or Cordón del Portillo). Our data definitively demonstrates the continuity of exhumation across the flat slab transition with the additional constraint of AFT track lengths that indicate rapid cooling initiated at ca. 16 Ma, and agree with independent geological evidence (Porras et al., 2016; Pinto et al., 2018; Buelow et al., 2018). The estimated lag-time derived average exhumation rate from ~16 Ma to recent (~200-275 m/Myr) is consistent with tectonically active orogens (for which rates may vary between 100-1000 m/Myr; e.g., Burbank, 2002; Montgomery and Brandon, 2002), and is comparable to that obtained by Riesner et al. (2019) for Cordón del Portillo using an AHe vertical sampling profile, as well as decadal and millennial scale erosion rates for the Frontal Cordillera (Carretier et al., 2013; Pepin et al., 2013; Val et al., 2018) over the same range of latitudes.

5.2 Regional integration of thermochronologic, structural and stratigraphic results

The recent spate of new geochronology and provenance results from synorogenic basins (Buelow et al., 2018; Pinto et al., 2018; Porras et al., 2016), bedrock and detrital thermochronology results (this study, Riesner et al., 2019; Hoke et al., 2015), as well as our field observations demonstrates that rock uplift and exhumation of the Frontal Cordillera initiated during the early Miocene. By spanning the flat slab transition, our detrital fission track dataset helps unify this result over ~ 3° of latitude to clearly refute the long-held view that the onset of deformation of the Frontal Cordillera was linked to the Pampean flat slab (initiated at ~11 Ma at the latitude of 33°S, Yañez et al., 2002; Ramos et al., 2009).

The proposed ca. 16 Ma rock uplift and exhumation pulse for the Cordón del Plata and northern sector of Cordón del Portillo is nearly synchronous with evidence of contractional deformation of the Frontal Cordillera range occurring at different latitudes along the

structural trend (Fig. 7). At 30°S, structural analyses (Giambiagi et al., 2017) and bedrock AFT thermochronology (Lossada et al., 2017; Rodriguez et al., 2018) constrain a phase of Miocene mountain building beginning at ca. 18 Ma. At 31°S, stratigraphic, geochronologic and thermochronologic analysis of the foreland basin (Levina et al., 2014) indicate that significant exhumation of the Frontal Cordillera occurred at ca. 17 Ma. At the Manantiales Basin (32ºS, Fig. 7), new geochronology (Mazzitelli et al., 2015; Pinto et al., 2018) points towards an onset of Miocene deformation also ca. 16 Ma. Integrating these previous results for the timing of rock uplift and exhumation of Frontal Cordillera at different latitudes with the data presented here, it is evident that the traditional model of diachronous north to south deformation tracking the southward sweep of the subducting Juan Fernandez Ridge, and presumed flat slab during the Miocene (Ramos et al., 2002; Giambiagi and Ramos, 2002; Yáñez et al., 2001) does not apply to the Frontal Cordillera (Fig. 7). This observation is also valid for the beginning of deformation of the Precordillera, which is nearly synchronous at ca. 13 Ma along its structural strike (Walcek and Hoke, 2012; Levina et al., 2014; Suriano et al., 2017, Buelow et al., 2018, Fig. 7), rejecting a north-to-south progression of deformation. Moreover, our data suggest that the main period of rock uplift and exhumation of the Frontal Cordillera at the study latitude, and all along its structural extent, based on the available evidence, pre-dates the beginning of flat slab conditions (Yañez et al., 2001), and instead are likely the result of compressional stresses in a normal subduction geodynamic context. In this scenario, upper crustal shortening resulted in crustal thickening beneath the Principal Cordillera (~20 to 9 Ma, Ramos et al., 2002) until a threshold value is achieved (i.e., Giambiagi et al., 2015). The gravitational forces created by the buoyant crustal root exceed the driving tectonic forces, forcing lateral growth instead of vertical growth of the orogen (Molnar and Lyon-Caen, 1988), to lower the taper by propagating foreland-ward. As a result, thrusting shifted eastward and a new, deeper decollement (Fig. 1c and 1d) formed in the east,

uplifting the basement blocks of Frontal Cordillera (~16 Ma). Although many studies have shown that plate-scale changes in the rate and direction of relative convergence between the Nazca (or Farallones) and the South America plates and/or in the absolute velocity of South America correlate with major episodes of deformation in the overriding plate (Pardo-Casas and Molnar, 1987; Somoza, 1998; Silver et al., 1998; Sobolev and Babeyko, 2005; Oncken et al., 2006; Horton, 2018, among others), no consensus exists regarding which parameter dominates.

Maloney et al. (2013) resolved the subduction parameters of the Andean margin since the Jurassic applying a kinematic global plate model, and analyzed their link with the style of deformation of the upper plate. They concluded that fold and thrust belts generally developed under trench normal convergence velocities greater than 4 cm/yr, but sometimes that threshold value is reached prior to the development of contractional features on the overriding plate, indicating that other factors are necessary as well. The proposed regional event of contractional deformation of the Frontal Cordillera at ca. 16 Ma correlates with a progressive decay in convergence velocity between the Nazca and South America plates, from its maximum value during the Cenozoic between ~28 and 25 Ma of ~15 cm/yr (Somoza, 1998), and with a diminished to nearly invariant trench-normal absolute South American plate velocity of ~1 cm/yr for the last 20 Myr (Maloney et al., 2013). Whereas no clear correlation can be made between convergence velocity or westward absolute South America velocity and the 15.3-17 Ma regional exhumation signal we observe, there is a marked change in mean convergence azimuth between Nazca and the South America plates from N69°E to N82°E (Somoza, 1998). This change to a more orthogonal collision, together with favorable values of relative convergence velocities and the achievement of a threshold value of crustal thickness in the arc region, may have promoted the development of the Frontal Cordillera thick-skinned fold and thrust belt and associated regional exhumation.

Finally, the integration of structural, stratigraphic, and thermochronologic results for the different morphostructural units composing the Andes at 33ºS, as shown in figure 6, demonstrates that the locus of Neogene shortening has advanced eastward, from the Aconcagua fold-and-thrust belt (~20-8 Ma, Ramos et al., 1996, Fig. 6), Frontal Cordillera (15.3-17 Ma, Buelow et al., 2018, this study), Precordillera (~12 Ma, Buelow et al., 2018) and the broken foreland (<5 Ma, Ramos et al., 2002), refuting recent studies that postulate a west-advancing tectonic model for the Andes at ~33ºS (Armijo et al., 2010; Riesner et al., 2017, 2018, 2019). The WAT west-vergent orogenic model proposed by Riesner et al. (2019) for the Andes at the latitude of ~33.5ºS requires that the Frontal Cordillera uplifts (and is exhumed) first, in the late Oligocene to early Miocene (20-25 Ma) and sustains the deformation until present, which contradicts (i) timing of deformation in Aconcagua belt, sealed by the ~16 Ma horizontal volcanic rock from the Aconcagua volcano, (ii) provenance analysis both from the Alto Tunuyán and Cacheuta Miocene basins, (iii) eastward-vergent uplift of the Cordón del Plata, exposing Proterozoic rocks in its easternmost sector, (iv) 2-km topographic uplift of the intermontane Alto Tunuyán basin after 9 Ma, and (v) along strike thermochronology data and proposed eastward advance of deformation from this study.

6 Conclusions

Detrital fission-track thermochronology provides valuable information to the study of the deformational history of the Frontal Cordillera range between 32°40´ and 33°40´S, in an area of difficult access. A consistent AFT age mode of 15.3-17 Ma was present in all samples from the Cordón del Plata and northern sector of Cordón del Portillo. Fission track lengths from the one sample (A13-15) that had a single peak at 17.0 ± 1.1 Ma indicated that rocks cooled rapidly through the partial annealing zone. We interpret this rapidly cooling episode at ~16 Ma as direct evidence for exhumation in the Frontal Cordillera blocks. This

interpretation is in good agreement with other independent evidence involving sedimentological, provenance and paleotopography analysis in the Cacheuta and Alto Tunuyán synorogenic basins. Exhumation of the Cordón del Plata and northern sector of the Cordón del Portillo is due to reverse fault activity along the NNE-striking La Carrera fault system. Constraining significant early to middle Miocene rock uplift and exhumation of the Frontal Cordillera, previously unrecognized in the area, allows evaluation of the classic model of Miocene Andean evolution at 33ºS, in which deformation shifted eastward into Frontal Cordillera at 9 Ma, in response to the flattening of the slab since ca. 11 Ma. As the main rock uplift pulse of Frontal Cordillera at ca. 16 Ma predates the development of flat slab conditions at 33ºS, integrating our data with previous studies at different latitudes, permits the rejection of the prevailing tectonic model of a north-to-south migration of the Frontal Cordillera deformation. Instead, we propose Frontal Cordillera Miocene rock uplift and exhumation occurred during a normal subduction regime, under favorable relative convergence velocity and convergence obliquity conditions and potentially followed the achievement of a threshold value of crustal thickness in the arc region. Our data support an eastward sequential propagation of deformation of the morphostructural units present at the study latitude (Principal Cordillera, Frontal Cordillera and Precordillera). This strengthens the tectonic model for an east-vergent mountain belt.

Acknowledgments

We would like to thank reviewers Mauricio Parra, Mark Brandon and Nick Pérez, and Associate Editor Marcelo Farías, who provided very helpful comments that greatly improved the present work. Lossada also acknowledges Victor Ramos for stimulating discussions. This research was supported by an Argentine Presidential- Fulbright Fellowship in Science and Technology for Lossada's 9 months in residence at Syracuse University during 2015–2016 and the Argentine Foncyt PICT-2011-1079 and PICT-2016-0269 projects. Hoke acknowledges support of the Donors of the American

Chemical Society's Petroleum Research Fund for award 52480-DNI8. All of the data have been archived at the Geochron data base (https://www.geochron.org/dataset/html/geochron_dataset_2019_11_27_h06d4)

References

Anderson, M., Alvarado, P., Zandt, G., Beck, S.L. (2007), Geometry and brittle deformation of the subducting Nazca Plate, central Chile and Argentina: *Geophysical Journal International* 171(1), 419–434.

Armijo, R., Rauld, R., Thiele, R., Vargas, G., Campos, J., Lacassin, R., Kausel, E. (2010), The West Andean Thrust, the San Ramón Fault, and the seismic hazard for Santiago, Chile. *Tectonics* 29, TC2007. https://doi.org/10.1029/2008TC002427

Baldwin, S.L., Harrison, T.M., Burke, K. (1986), Fission track evidence for the source of Scotland District sediments, Barbados and implications for post-Eocene tectonics of the southern Caribbean. *Tectonics* 5, 457–468

Barazangi, M., and Isacks, B. L. (1976), Spatial distribution of earthquakes and subduction of the Nazca plate beneath South America. *Geology 4*(11), 686-692.

Bernet, M. (2019), Chapter 15 Exhumation studies of mountain belts based on detrital fission-track analysis on sand and sandstones. In: Malusà MG, Fitzgerald PG (Eds) *Fission-track thermochronology and its application to geology*. P. 269-277. Springer. doi.org/10.1007/978-3-319-89421-8_15.

Bernet, M., Zattin, M., Garver, J. I., Brandon, M. T., Vance, J. A. (2001), Steady-state exhumation of the European Alps. *Geology*, *29*(1), 35-38.

Bernet, M., Brandon, M. T., Garver, J. I., Molitor, B. R. (2004), Fundamentals of detrital zircon fission-track analysis for provenance and exhumation studies with examples from the European Alps. *Geological Society of America, Special Papper*, 25-36.

Brandon, M.T. and Vance, J.A. (1992), Tectonic evolution of the Cenozoic Olympic Subduction Complex, Washington State, as deduced from fission-track ages for detrital zircons. *American Journal of Science* 292:565–636.

Brandon, M. T., Roden-Tice, M. K., and Garver, J. I. (1998), Late Cenozoic exhumation of the Cascadia accretionary wedge in the Olympic Mountains, northwest Washington State. *Geological Society of America Bulletin*, *110*(8), 985-1009.

Braun, J., Van Der Beek, P., and Batt, G. (2006), *Quantitative thermochronology: numerical methods for the interpretation of thermochronological data*. Cambridge University Press.

Brewer, I. D., Burbank, D. W., and Hodges, K. V. (2003), Modelling detrital cooling-age populations: insights from two Himalayan catchments. *Basin Research*, *15*(3), 305-320.

Brooks, B. A., Bevis, M., Smalley Jr, R., Kendrick, E., Manceda, R., Lauría, E., ... & Araujo, M. (2003). Crustal motion in the Southern Andes (26°–36° S): Do the Andes behave like a microplate?. *Geochemistry, Geophysics, Geosystems*, *4*(10).

Buelow, E. K., Suriano, J., Mahoney, J. B., Kimbrough, D. L., Mescua, J. F., Giambiagi, L. B., Hoke, G. D. (2018), Sedimentologic and stratigraphic evolution of the Cacheuta

basin: Constraints on the development of the Miocene retroarc foreland basin, south-central Andes. *Lithosphere*, *10*(3), 366-391.

Burbank, D.W. (2002), Rates of erosion and their implications for exhumation. *Min Mag* 66:25-52.

Cahill, T. and Isacks, B. L. (1992), Seismicity and shape of the subducted Nazca plate. *Journal of Geophysical Research* 97: 17503-17529.

Caminos, R. (1964), Estratigrafía y tectónica del Espolón de la Carrera, Cordón del Plata, provincia de Mendoza. PhD Thesis, Universidad Nacional de Buenos Aires, 145 p., Buenos Aires.

Caminos, R. (1965), Geología de la vertiente oriental del Cordón del Plata, Cordillera Frontal de Mendoza. *Revista de la Asociación Geológica Argentina* 20(3): 351-392.

Carrasquero, S. I., Rubinstein, N. A., Gómez, A. L., Chiaradia, M., Fontignie, D., & Valencia, V. A. (2018). New insights into petrogenesis of Miocene magmatism associated with porphyry copper deposits of the Andean Pampean flat slab, Argentina. *Geoscience Frontiers*, *9*(5), 1565-1576.

Carretier, S., Regard, V., Vassallo, R., Aguilar, G., Martinod, J., Riquelme, R., ... & Guyot, J. L. (2013). Slope and climate variability control of erosion in the Andes of central Chile. Geology, 41(2), 195-198.

Casa, A. L. (2005), Geología y neotectónica del piedemonte oriental del Cordón del Plata en los alrededores de El Salto. Thesis degree, Universidad de Buenos Aires, 174 p., Buenos Aires.

Casa, A. L., Borgnia, M. M. and Cortés, J. M. (2010), Evidencias de deformación pleistocena en el sistema de falla de La Carrera (32º40'-33º15' LS), Cordillera Frontal de Mendoza. *Revista de la Asociación Geológica Argentina* 67: 91-104.

Cegarra, M., Ramos, V. (1996), La faja plegada y corrida del Aconcagua. In Ramos, V. (Ed.) *Geologia de la Region del Aconcagua*, Direccion Nacional del Servicio Geologico, Buenos Aires, 24: 386-422

Cerveny, P.F., Naeser, N.D., Zeitler, P.K., Naeser, C.W., Johnson, N.M. (1988), History of uplift and relief of the Himalaya during the past 18 million years: evidence from sandstones of the Siwalik group. In: Kleinspehn, K.L and Paola, C. (eds.) *New Perspectives in Basin Analysis*, Springer: 43–61, New York.

Charrier, R., Pinto, L. and Rodríguez, M. (2007), Tectonostratigraphic evolution of the Andean Orogen in Chile. In Moreno, T. and Gibbons, W. (eds.). *The Geology of Chile*, Geological Society: 21-114, London.

Charrier, R., Baeza, O., Elgueta, S., Flynn, J. J., Gans, P., Kay, S. M., ... and Zurita, E. (2002), Evidence for Cenozoic extensional basin development and tectonic inversion south of the flat-slab segment, southern Central Andes, Chile (33–36 SL). *Journal of South American Earth Sciences*, *15*(1), 117-139.

Cortés, J. M. (1993), El frente de la Cordillera Frontal y el extremo sur del valle de Uspallata, Mendoza. XII Congreso Geológico Argentino, Actas: 168-178, Mendoza.

Cristallini, E. O., & Ramos, V. A. (2000). Thick-skinned and thin-skinned thrusting in the La Ramada fold and thrust belt: crustal evolution of the High Andes of San Juan, Argentina (32 SL). *Tectonophysics*, *317*(3-4), 205-235.

Farías, M., Charrier, R., Carretier, S., Martinod, J., Fock, A., Campbell, D., Cáceres, J., Comte, D. (2008), Late Miocene high and rapid surface uplift and its erosional response in the Andes of central Chile (33–35 S). *Tectonics*, 27(1).

Farías, M., Comte, D., Charrier, R., Martinod, J., David, C., Tassara, A., ... & Fock, A. (2010). Crustal-scale structural architecture in central Chile based on seismicity and surface geology: Implications for Andean mountain building. *Tectonics*, *29*(3).

Fauqué, L., Cortés, J. M., Folguera, A., Etcheverría, M. (2000), Avalanchas de rocas asociadas a neotectónica en el valle del río Mendoza, al sur de Uspallata. *Revista de la Asociación Geológica Argentina* 55: 419-423.

Folguera, A., Etcheverria, M., Pazos, P., Giambiagi, L., Cortés, J. M., Fauqué, L., Fusari, C., Rodríguez, M. F. (2004), Descripción de la Hoja Geológica N° 3369-15 (Potrerillos). Carta Geologica de la República Argentina E. 1:100.000. Subsecretaría de Minería de la Nación, Dirección Nacional del Servicio Geológico, 262 p.

Fosdick, J. C., Carrapa, B., & Ortíz, G. (2015). Faulting and erosion in the Argentine Precordillera during changes in subduction regime: Reconciling bedrock cooling and detrital records. *Earth and Planetary Science Letters*, *432*, 73-83.

Galibraith, R. F. and Green, P. F. (1990), Estimating the component ages in a finite mixture. *Nuclear Tracks and Radiation Measurement*, 17: 197-206.

Gallagher, K., Brown, R., and Johnson, C. (1998), Fission track analysis and its applications to geological problems, *Annual Review of Earth and Planetary Sciences* 26:519-572

Gans, C. R., Beck, S. L., Zandt, G., Gilbert, H., Alvarado, P., Anderson, M., Linkimer, L. (2011), Continental and oceanic crustal structure of the Pampean flat slab region, western Argentina, using receiver function analysis: new high-resolution results. *Geophysical Journal International*, *186*(1), 45-58.

Garver, J. I., Brandon, M. T., Roden-Tice, M., Kamp, P. J. (1999) Exhumation history of orogenic highlands determined by detrital fission-track thermochronology. *Geological Society, London, Special Publications*, *154*(1), 283-304.

Giambiagi, L. (1999), Los depósitos neógenos de la región del río Palomares, Cordillera Principal de Mendoza, *Revista Asociacion Geologica Argentina*, 54 (1): 47-59

Giambiagi, L. (2000), Estudio de La evolución tectónica de la Cordillera Principal de Mendoza en el sector comprendido entre los 33°30′ y los 33°45′ Latitud Sur (Ph.D. thesis) Universidad de Buenos Aires (2000) (255 p)

Giambiagi, L. B., & Ramos, V. A. (2002). Structural evolution of the Andes in a transitional zone between flat and normal subduction (33 30′–33 45′ S), Argentina and Chile. *Journal of South American Earth Sciences*, *15*(1), 101-116.

Giambiagi, L. B., Tunik, M. and Ghiglione, M. (2001), Cenozoic tectonic evolution of the Alto Tunuyán foreland basin above the transition zone between the flat and normal subduction segment (33°30´ –34°S), western Argentina. *Journal of South America Earth Sciences*, 14: 707 – 724.

Giambiagi, L., V.A. Ramos, E. Godoy, P.P. Álvarez, Orts, S. (2003), Cenozoic deformation and tectonic style of the Andes, between 33° and 34° South Latitude, *Tectonics*, 22 (4) p. 1041, 10.1029/2001TC001354

Giambiagi, L., Mescua, J., Bechis, F., Martínez, A., Folguera, A. (2011), Pre-Andean deformation of the Precordillera southern sector, Southern Central Andes. *Geosphere*, 7: 219-239

Giambiagi, L., Mescua, J., Heredia, N., Farías, P., García Sansegundo, J., Fernández, C., Stier, S., Pérez, D., Bechis, F., Moreiras, S. M., Lossada, A. (2014), Reactivation of Paleozoic structures during Cenozoic deformation in the Cordón del Plata and Southern Precordillera ranges (Mendoza, Argentina). *Journal of Iberian Geology* 40(2): 309-320.

Giambiagi, L., Tassara, A., Mescua, J., Tunik, M., Alvarez, P., Godoy, E., … Pagano, S. (2015). Evolution of shallow and deep structures along the Maipo-Tunuyán transect (33°40´S): From the Pacific coast to the Andean foreland. In S. A. Sepúlveda, et al. (Eds.), *Geodynamic Processes in the Andes of Central Chile and Argentina. Geological Society of London Special Publication*, 339, 63–82

Giambiagi, L., Álvarez, P. P., Creixell, C., Mardonez, D., Murillo, I., Velásquez, R., ... & Barrionuevo, M. (2017). Cenozoic Shift From Compression to Strike-Slip Stress Regime in the High Andes at 30° S, During the Shallowing of the Slab: Implications for the El Indio/Tambo Mineral District. *Tectonics*, *36*(11), 2714-2735

Gallagher, K., and Parra, M. (2020). A new approach to thermal history modelling with detrital low temperature thermochronological data. Earth and Planetary Science Letters, 529, 115872

Gleadow, A.J.W. and Duddy, I.R. (1981), A natural long term annealing experiment for apatite. *Nucl.Tracks* 5:169–74

Green, P. F. (1981). A new look at statistics in fission track dating. Nuclear Tracks and Radiation Measurements, 5(1–2), 77–86. https://doi.org/10.1016/0191-278X(81)90029-9

Green, P. F., Duddy, I. R., Laslett, G. M., Hegarty, K. A., Gleadow, A. W., Lovering, J. F. (1989), Thermal annealing of fission tracks in apatite 4. Quantitative modelling techniques and extension to geological timescales. *Chemical Geology: Isotope Geoscience Section*, *79*(2), 155-182.

Gutscher, M.A., Spakman,W., Bijwaard, H., Engdahl, E.R., (2000), Geodynamics of flat slab subduction: Seismicity and tomographie constraints from the Andean margin. *Tectonics* 19 (5): 814-833.

Heredia, N., Farías, P., García Sansegundo, J., Giambiagi, L. (2012), The basement of the Andean Frontal Cordillera in the Cordón del Plata (Mendoza, Argentina): geodynamic evolution. *Andean Geology* 39: 242-257.

Hoke, G. D., Giambiagi, L. B., Garzione, C. N., Mahoney, J. B., Strecker, M. R. (2014), Neogene paleoelevation of intermontane basins in a narrow, compressional mountain range, southern Central Andes of Argentina. *Earth and Planetary Science Letters*, *406*, 153-164.

Hoke, G., Graber, N., Mescua, J., Giambiagi, L., Fitzgerald, P., Metcalf, J. (2015), Near pure surface uplift of the Argentine Frontal Cordillera: insights from (U-Th)/He thermochronometry and geomorphic analysis. In Sepúlveda et al. (eds) *Geodynamic Processes in the Andes of Central Chile and Argentina*, Geological Society of London Special Publication 339, London.

Horton, B. K. (2018), Tectonic regimes of the central and southern Andes: responses to variations in plate coupling during subduction. *Tectonics*, *37*(2), 402-429.

Horton, B. K., and Fuentes, F. (2016), Sedimentary record of plate coupling and decoupling during growth of the Andes. *Geology*, *44*(8), 647-650.

Hurford, A.J. (1990), Standardization of ission-track dating calibration: recommendation by the ission track working group of the I.U.G.S. subcommission on geochronology. *Chem Geol* 80:171–178

Hurford, A.J. and Green, P.F. (1982), A users' guide to ission-track dating calibration. *Earth Planetary Sciences Letters* 59:343–354

Irigoyen, M. V. (1997), Magnetic polarity stratigraphy and geochronological constraints on the sequence of thrusting in the Principal and Frontal cordilleras and the Precordillera of the Argentine Central Andes (33° S latitude). Ph.D. thesis, Carleton University, 392 p., Ottawa.

Irigoyen, M. V., Buchan, K. L. and Brown, R. L. (2000), Magnetostratigraphy of Neogene Andean foreland-basin strata, lat 33°S, Mendoza province, Argentina. *Geological Society of America Bulletin* 112: 803-816.

Isacks, B.L., 1988, Uplift of the Central Andean Plateau and bending of the Bolivian Orocline: Journal of Geophysical Research, v. 93, p. 3211-3231.

Isacks, B. L., and Barazangi, M. (1977), Geometry of Benioff zones: Lateral segmentation and downwards bending of the subducted lithosphere. *Island Arcs, Deep Sea Trenches and Back-Arc Basins*, *1*, 99-114.

Jara, P., Likerman, J., Winocur, D., Ghiglione, M., Cristalini, E., Pinto, L., Charrier, R. (2015), Role of basin width variation in tectonic inversion: insight from analogue modeling and implications for the tectonic inversion of the Abanico Basin, 32°-34°S, Central Andes. In Sepúlveda et al. (Eds.) *Geodynamic Processes in the Andes of Central Chile and Argentina, Geological Society of London, Special Publication,* 339: 83-107

Jordan, T., Isacks, B. L., Allmendinger, R. W., Brewer, J. A., Ramos, V. A., Ando, C. J. (1983), Andean tectonics related to geometry of subducted Nazca Plate. *Geological Society of America Bulletin* 94: 341–361.

Kay, S. M., Maksaev, V., Moscoso, R., Mpodozis, C., Nasi, C., Gordillo, C. E. (1987), Tertiary Andean magmatism in Chile and Argentina between 28°S and 33°S: correlation of magmatic chemistry with a changing Benioff zone. *Journal of South American Earth Sciences* 1(1): 21-38.

Kay, S. M., and Mpodozis, C. (2002), Magmatism as a probe to the Neogene shallowing of the Nazca plate beneath the modern Chilean flat-slab. *Journal of South American Earth Sciences*, *15*(1), 39-57.

Kleiman, L. E., & Japas, M. S. (2009). The Choiyoi volcanic province at 34 S–36 S (San Rafael, Mendoza, Argentina): Implications for the Late Palaeozoic evolution of the southwestern margin of Gondwana. Tectonophysics, 473(3-4), 283-299.

Kozlowski, E., Manceda, R., and Ramos, V. (1993), Estructura. En: Ramos V (Ed.) Geologia y recusros naturales de Mendoza. XII Cong Geol Arg 1(18): 235-256

Levina, M., Horton, B. K., Fuentes, F., Stockli, D. F., (2014), Cenozoic sedimentation and exhumation of the foreland basin system preserved in the Precordillera thrust belt (31–32° S), southern central Andes, Argentina: *Tectonics*, 33 (9): 1659-1680.

Lossada, A. C., Giambiagi, L., Hoke, G. D., Fitzgerald, P. G., Creixell, C., Murillo, I., ... and Suriano, J. (2017), Thermochronologic evidence for late Eocene Andean mountain building at 30 S. *Tectonics*, *36*(11), 2693-2713.

Mahoney, B., Buelow, E.K., Suriano, J., Kimbrough, D., Mescua, J., and Giambiagi, L., 2016, Tracking basin inversion in the retroarc foreland basin: Integrated provenance studies in the Cacheuta basin, south-central Andes, in Proceedings of the 35th International Geological Congress: Capetown, South Africa, International Geological Congress, Abstract T29.6:5110

Malusà, M.G. and P.G. Fitzgerald, (2019a*), Fission track thermochronology and its application to geology.* Springer. doi.org/10.1007/978-3-319-89421-8. 393 p.

Malusà, M.G. and P.G. Fitzgerald, (2019b), Application of thermochronology to geologic problems: Approaches and conceptual models. In: Malusà, M.G. and P.G. Fitzgerald (eds.), *Fission track thermochronology and its application to geology*, p. 191-209, Springer, doi.org/10.1007/978-3-319-89421-8_10.

Malusà, M. G., Resentini, A., and Garzanti, E. (2016), Hydraulic sorting and mineral fertility bias in detrital geochronology. *Gondwana Research*, *31*, 1-19.

Mazzitelli, M., Mahoney, B., Balgord, E., Giambiagi, L., Kimbrough, D., Lossada, A., Maccann, C. (2015), Evolution of the Manatiales Basin, San Juan, Argentina: constraining Miocene orogenic patterns in the South-Central Andes. GSA Meet 47(7): 151

Mescua, J.F., Mahoney, J.B., Suriano, J., Vera, B., Kimbrough, D.L., Giambiagi, L.B., Cerdeño, E., and Buelow, E., 2017, Edad U-Pb de la Formación Divisadero Largo y consideraciones paleoambientales: XX Congreso Geológico Argentino, Actas, v. S9, p. 31–32.

Montgomery, D.R., and Brandon, M.T. (2002), Topographic controls on erosion rates in tectonically active mountain ranges. *Earth Planet Sci Lett* 201:481-489

Mpodozis, C. and Ramos, V. (1989), The Andes of Chile and Argentina. In Ericksen G E, Cañas Pinochet M T, Reinemund J A (eds.) Geology of the Andes and Its Relation to Hydrocarbon and Mineral Resources. Circum-Pacific Council for Energy and Mineral Resources, Houston, Texas, pp.56–90.

Naipauer, M., Tapia, F., Mescua, J.F., Farías, M., Pimentel, M.M., Ramos, V.A., (2015), Detrital and volcanic zircon U-Pb ages from southern Mendoza (Argentina): an insight on the source regions in the northern part of Neuquén Basin. *Journal of South American Earth Sciences*. doi:10.1016/j.jsames.2015.09.013

Nyström. J.O., Vergara, M., Morata, D., Levi, B. (2003), Tertiary volcanism during extension in the Andean foothills of central Chile (33°15′–33°45′S). *GSA Bulletin*, 115 (12): 1523-1537. doi: 10.1130/B25099.1.

Oliveros, V., Morata, D., Aguirre, L., Féraud, G., Fornari, G. (2007), Jurassic to Early Cretaceous subduction-related magmatism in the Coastal Cordillera of northern Chile (18°30'-24°S): geochemistry and petrogenesis. *Revista Geológica de Chile* 34(2): 209-232.

Oncken, O., Hindle, D., Kley, J., Elger, K., Victor, P., Schemmann, K. (2006), Deformation of the central Andean upper plate system—Facts, fiction, and constraints for plateau models. In *The Andes* (pp. 3-27). Springer, Berlin, Heidelberg.

Pardo-Casas, F. and Molnar, P. (1987), Relative motion of the Nazca (Farallon) and South American plates since late Cretaceous time. *Tectonics* 6(3): 233-248.

Pepin, E., Carretier, S., Hérail, G., Regard, V., Charrier, R., Farías, M., Garcia, V., Giambiagi, L. (2013). Pleistocene landscape entrenchment: a geomorphological mountain to foreland field case, the Las Tunas system, Argentina. *Basin Research*, *25*(6), 613-637.

Pilger, R. H. (1984), Cenozoic plate kinematics, subduction and magmatism: South American Andes. *Journal of Geolical Society of America* 141(5): 793-802.

Pinto, L., Alarcón, P., Morton, A., & Naipauer, M. (2018). Geochemistry of heavy minerals and U–Pb detrital zircon geochronology in the Manantiales Basin: Implications for Frontal Cordillera uplift and foreland basin connectivity in the Andes of central Argentina. *Palaeogeography, palaeoclimatology, palaeoecology*, *492*, 104-125.

Polanski, J. (1957), El bloque varíscico de la Cordillera Frontal de Mendoza. *Revista de la Asociación Geológica Argentina* 12(3): 165-196.

Polanski, J. (1964), Descripción geológica de la Hoja 25a, Volcán San José, provincia de Mendoza. Dirección Nacional de Geología y Minería, Boletín 98.

Polanski, J. (1972), Descripción geológica de la Hoja 24 a-b (Cerro Tupungato), provincia de Mendoza. Dirección Nacional de Geología y Minería, Buenos Aires, p 110

Porras, H., Pinto, L., Tunik, M., Giambiagi, L., and Deckart, K. (2016), Provenance of the Miocene Alto Tunuyán Basin (33° 40′ S, Argentina) and its implications for the evolution of the Andean Range: Insights from petrography and U–Pb LA–ICPMS zircon ages. *Tectonophysics*, *690*, 298-317.

Ramos, V.A. (1988), The tectonics of the Central Andes, 30° to 33°S latitude. In:Clark S, Burchfiel D (Eds.) Processes in continental lithospheric deformation: *Geological Society of America*, *Special Paper* 218: 31-54.

Ramos, V. A., & Folguera, A. (2009). Andean flat-slab subduction through time. *Geological Society, London, Special Publications*, *327*(1), 31-54.

Ramos, V. A., Cegarra, M. I. and Cristallini, E. (1996), Cenozoic tectonics of the High Andes of west-central Argentina (30°-36°S latitude). *Tectonophysics* 259: 185-200.

Ramos, V. A., Cristallini, E. and Pérez, D. (2002), The Pampean flat-slab of the Central Andes. *Journal of South American Earth Sciences* 15: 59-78.

Ramos, V., Aguirre-Urreta, M. B., Álvarez, P.P., Colluccia, A., Giambiagi, L., Pérez, D., Tunik, M., Vujovich, G. (2000), Descripción de la Hoja Geológica Cerro Tupungato, Provincia de Mendoza, 1:250.000. Subsecretaría de Minería de la Nación, Dirección Nacional del Servicio Geológico, Buenos Aires

Reiners, P. W. (2005), Zircon (U-Th)/He Thermochronometry. *Reviews in Mineralogy and Geochemistry* ; 58 (1): 151–179. doi: https://doi.org/10.2138/rmg.2005.58.6

Resentini, A., & Malusà, M. G. (2012). Sediment budgets by detrital apatite fission-track dating (Rivers Dora Baltea and Arc, Western Alps). *Geological Society of America Special Papers*, *487*, 125-140.

Riesner, M., Lacassin, R., Simoes, M., Carrizo, D., Armijo, R. (2018), Revisiting the Crustal Structure and Kinematics of the Central Andes at 33.5°S: Implications for the Mechanics of Andean Mountain Building, *Tectonics*, **37**(5):1347-1375.

Riesner, M., Lacassin, R., Simoes, M., Armijo, R., Rauld, R., Vargas, G. (2017), Kinematics of the active West Andean fold-and-thrust belt (central Chile): Structure and long-term shortening rate. *Tectonics*, 36, 287–303. https://doi.org/10.1002/2016TC004269

Riesner, M., Simoes, M., Carrizo, D., & Lacassin, R. (2019) Early exhumation of the Frontal Cordillera (Southern Central Andes) and implications for Andean mountain-building at~ 33.5 S. Scientific Reports, 9:7972, https://doi.org/10.1038/s41598-019-44320-1

Rodríguez, M. P., Charrier, R., Brichau, S., Carretier, S., Farías, M., de Parseval, P., Ketcham, R. A. (2018), Latitudinal and longitudinal patterns of exhumation in the Andes of north-central Chile. *Tectonics*.

Ruiz G, Seward D, Winkler W (2004) Detrital thermochronology–a new perspective on hinterland tectonics, an example from the Andean Amazon Basin, Ecuador. *Basin Res* 16: 413-430.

Silver, P. G., Russo, R. M., and Lithgow-Bertelloni, C. (1998), Coupling of South American and African plate motion and plate deformation. *Science* 279: 60-63

Sobolev, S. V., and Babeyko, A. Y., 2005, What drives orogeny in the Andes?: Geology, v. 33, n. 8, p. 617–620

Somoza, R. (1998), Updated Nazca (Farallon) - South America relative motions during the last 40 My: implications for mountain building in the central Andean region. *Journal of South American Earth Sciences*11(3): 211–215.

Suriano, J., Mardonez, D., Mahoney, J. B., Mescua, J. F., Giambiagi, L., Kimbrough, D., Lossada, A. (2017), Uplift sequence of the Andes at 30°S: Insights from sedimentology and U/Pb dating of synorogenic deposits. *Journal of South American Earth Sciences*, 75, 11–34.

Tunik, M. A. (2003). Interpretación paleoambiental de los depósitos de la Formación Saldeño (Cretácico superior), en la alta Cordillera de Mendoza, Argentina. *Revista de la Asociación Geológica Argentina*, *58*(3), 417-433.

Val, P., Hoke, G. D., Fosdick, J. C., Wittmann, H. (2016). Reconciling tectonic shortening, sedimentation and spatial patterns of erosion from 10Be paleo-erosion rates in the Argentine Precordillera. *Earth and Planetary Science Letters*, *450*, 173-185.

van der Beek, P., Robert, X., Mugnier, J.L., Bernet, M., Huyghe, P., Labrin, E. (2006), Late Miocene – Recent denudation of the central Himalaya and recycling in the foreland basin assessed by detrital apatite fission-track thermochronology of Siwalik sediments, Nepal. *Basin Res* 18, 413-434

Vermeesch, P. (2009), RadialPlotter: a Java application for fission track, luminescence and other radial plots. *Radiation Measurements*, 44 (4): 409-410.

Vermeesch, P., (2012), On the visualisation of detrital age distributions. *Chemical Geology*, 312-313: 190-194, doi: 10.1016/j.chemgeo.2012.04.021 0.

Walcek, A. A., and Hoke, G. D. (2012) Surface uplift and erosion of the southernmost Argentine Precordillera. *Geomorphology*, *153*, 156-168.

White, N.M., Pringle, M., Garzanti, E., Bickle, M., Najman, Y., Chapman, H., Friend, P. (2002), Constraints on the exhumation and erosion of the High Himalayan Slab, NW India, from foreland basin deposits. *Earth and Planetary Science Letters* 195: 29–44.

Willett, S. D., Fisher, D., Fuller, C., En-Chao, Y., Chia-Yu, L. (2003), Erosion rates and orogenic-wedge kinematics in Taiwan inferred from fission-track thermochronometry. *Geology*, *31*(11), 945-948.

Yáñez, G. A., Ranero, C. R., von Huene, R., Díaz, J. (2001), Magnetic anomaly interpretation across the southern central Andes (32°-34°S): The role of the Juan Fernandez Ridge in the late Tertiary evolution of the margin. *Journal of Geophysical Research* 106: 6325–6345.

Yáñez, G., Cembrano, J., Pardo, M., Ranero, C., Selles, D. (2002), The Challenger–Juan Fernandez–Maipo major tectonic transition of the Nazca-Andean subduction system at 33-34°S: geodynamic evidence and implications. *Journal of South American Earth Sciences* 15: 23-38.

Yrigoyen, M. R. (1993), Revisión estratigráfica del Neogeno de la region Cacheuta-La Pilona-Tupungato, Mendoza Septentrional, Argentina: XII Congreso Geológico Argentino y II Congreso de Exploración de Hidrocarburos. Actas, 2, 187-199.

Table 1: Best-fit age populations for apatite FTGA modern river samples, obtained with DensityPlotter (Vermeesch, 2012).

Sample	Lat (S)	Long (W)	N	P1		P2		P3		P4	
				Age (Ma)	Contrib (%)	Age (Ma)	Contrib(%)	Age (Ma)	Contrib(%)	Age (Ma)	Contrib(%)
A13-14 Arroyo Grande	33º35.8´	69º22.9´	97	15.3±1.1	24±5	57.7±5.2	23±11	110±11	22±7	187±13	31±7
A13-15 Las Tunas	33º28.4´	69º13.5´	99	17.0±1.1	100±0	–	–	–	–	–	–
A13-16 East Rio Blanco	32º57.9´	69º13.3´	83	15.6±1.7	23±5	84.2±6.2	44±7	198±16	33±8	–	–
A13-17 West Río Blanco	32º45.5´	69º34.9´	98	16.3±1.0	49.8±5.2	150±9	50.2±5.2	–	–	–	–

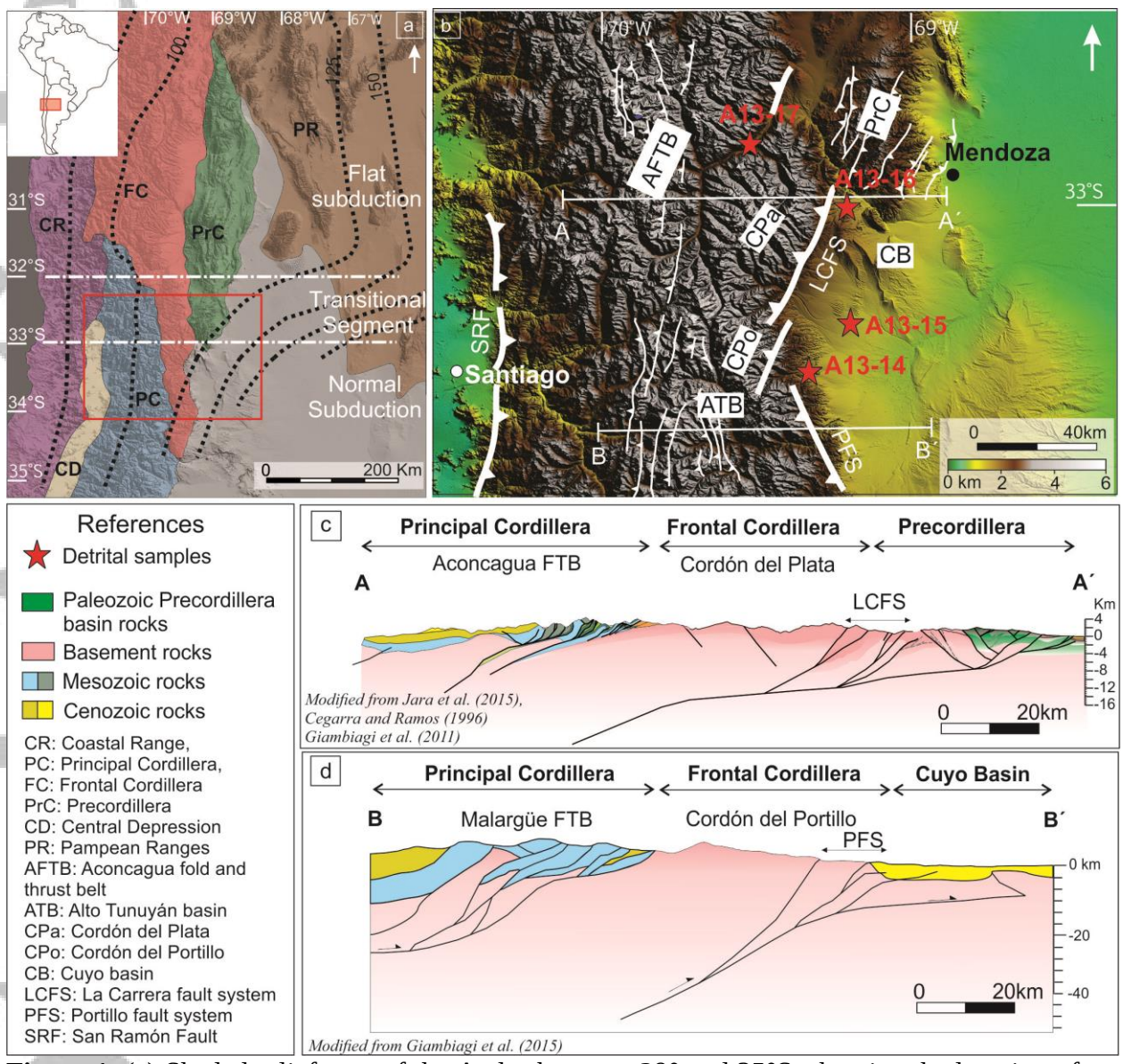

Figure 1: (a) Shaded relief map of the Andes between 29° and 35°S, showing the location of the study area (red rectangle). Dashed black lines indicate contours of the Wadatti-Benioff zone (Cahill and Isacks, 1992). (b) Topographic map of the study zone and sampling location (red stars). (c) and (d) Schematic structural profiles across the main morphotectonic units in the Cordón del Plata transect (c) and Cordón del Portillo transect (d). Location for each schematic cross section is shown in figure 1b.

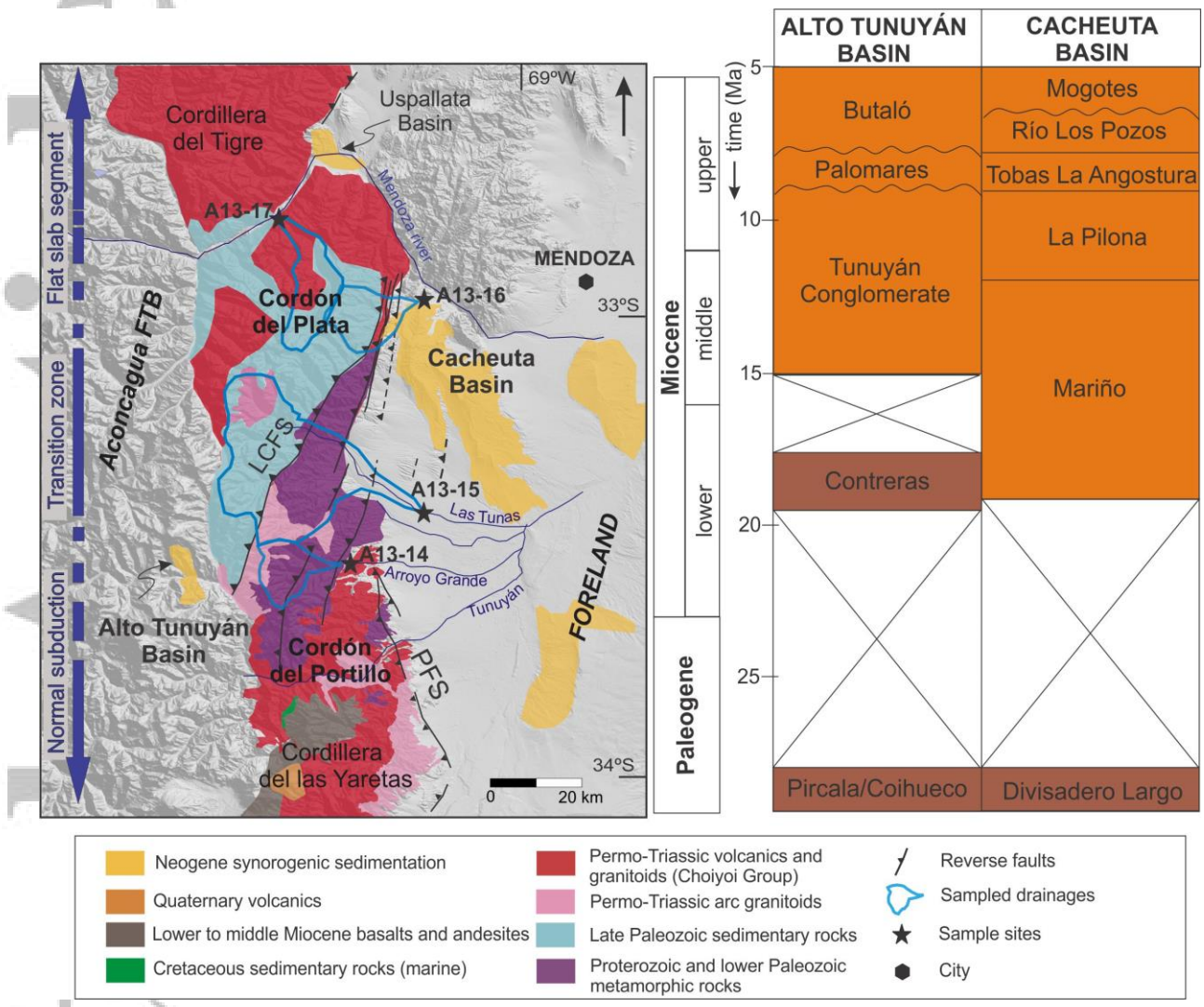

Figure 2: Geologic map and sampling areas (drainages). Stratigraphic chart of syntectonic Miocene basins.

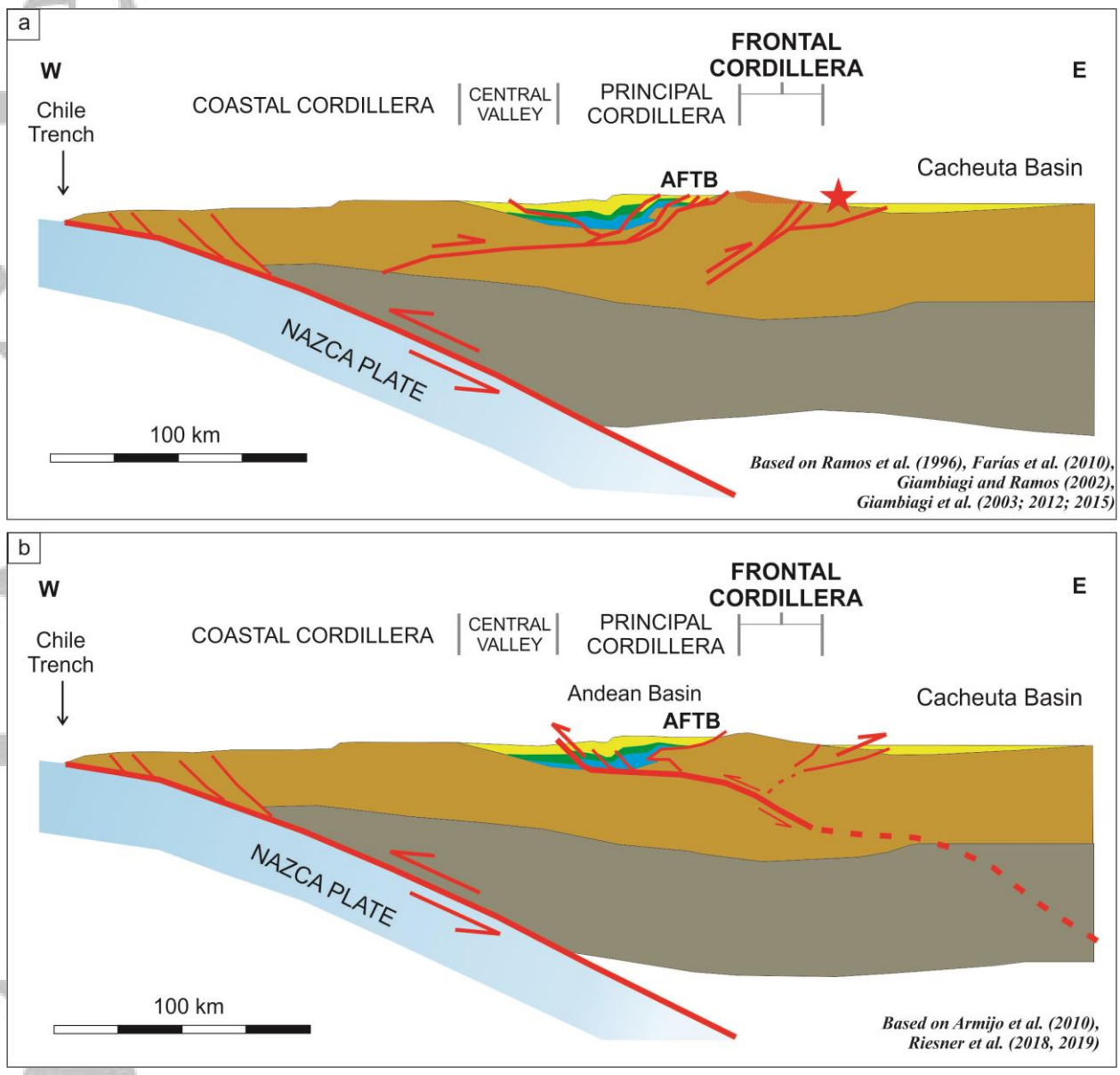

Figure 3: Schematic tectonic models proposed for the Andes at the latitude of ~33.5°S. (a) Traditional east-vergent orogenic model with and eastward sequential propagation of deformation. Approximately sampling location (red star) and corresponding sampled area is shown. (b) West-vergent orogenic model. Deformation is sustained along a west-vergent detachment, with an initial exhumation of Frontal Cordillera.

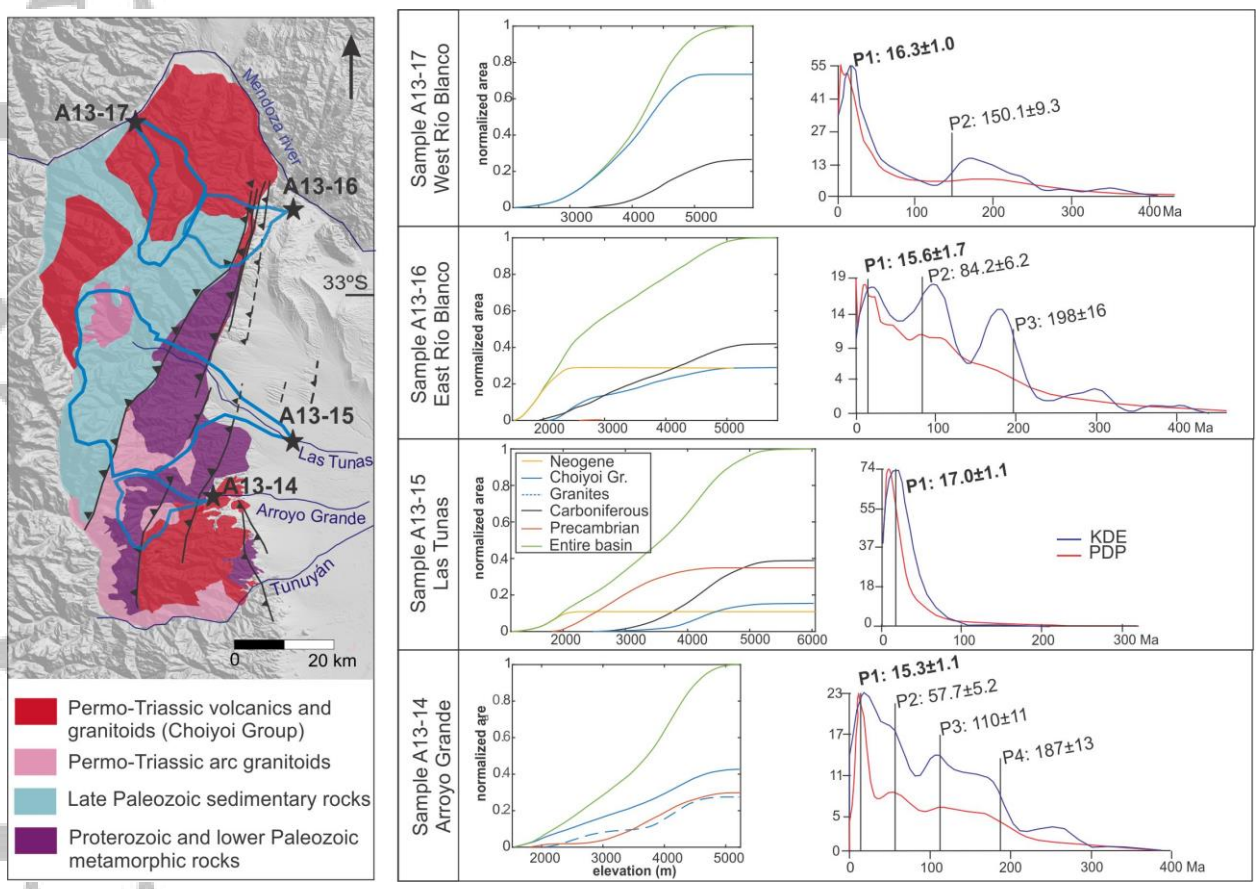

Figure 4: Hypsometric curves showing the distribution of lithologies in each catchment. Elevations were extracted from 90 m SRTM topography, binned at 35 m intervals to construct individual curves. Probability density plots (PDP) and kernel density estimates (KDE) showing the obtained cooling age modes at the different catchment are presented.

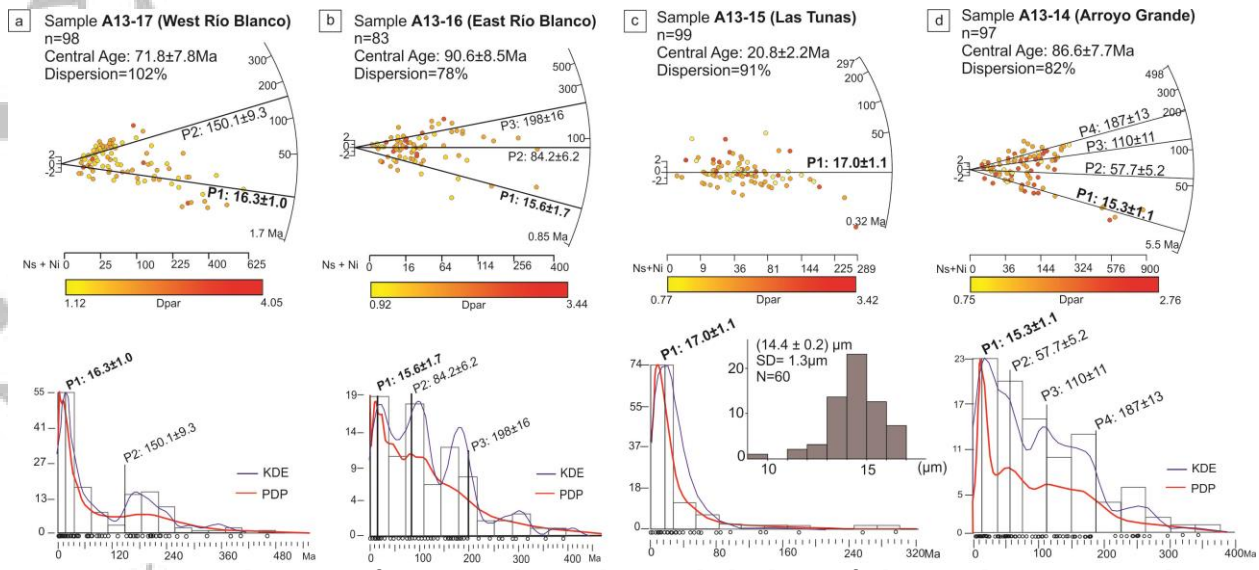

Figure 5: Detrital apatite fission-track results. Radial plots of the single-grain age data (above) and probability density plots (PDP) and kernel density estimate (KDE) (below) of fission-track grain-age distributions (3a, 3b, 3c and 3d) for samples A13-17, A13-16, A13-15 and A13-14, respectively. In the KDE the "kernel" was chosen to be Gaussian and a fixed bandwidth of 15 Track length distribution of sample A13-15 is shown in (3c) indicating mean length, standard deviation (SD) and number of confined tracks measured (N).

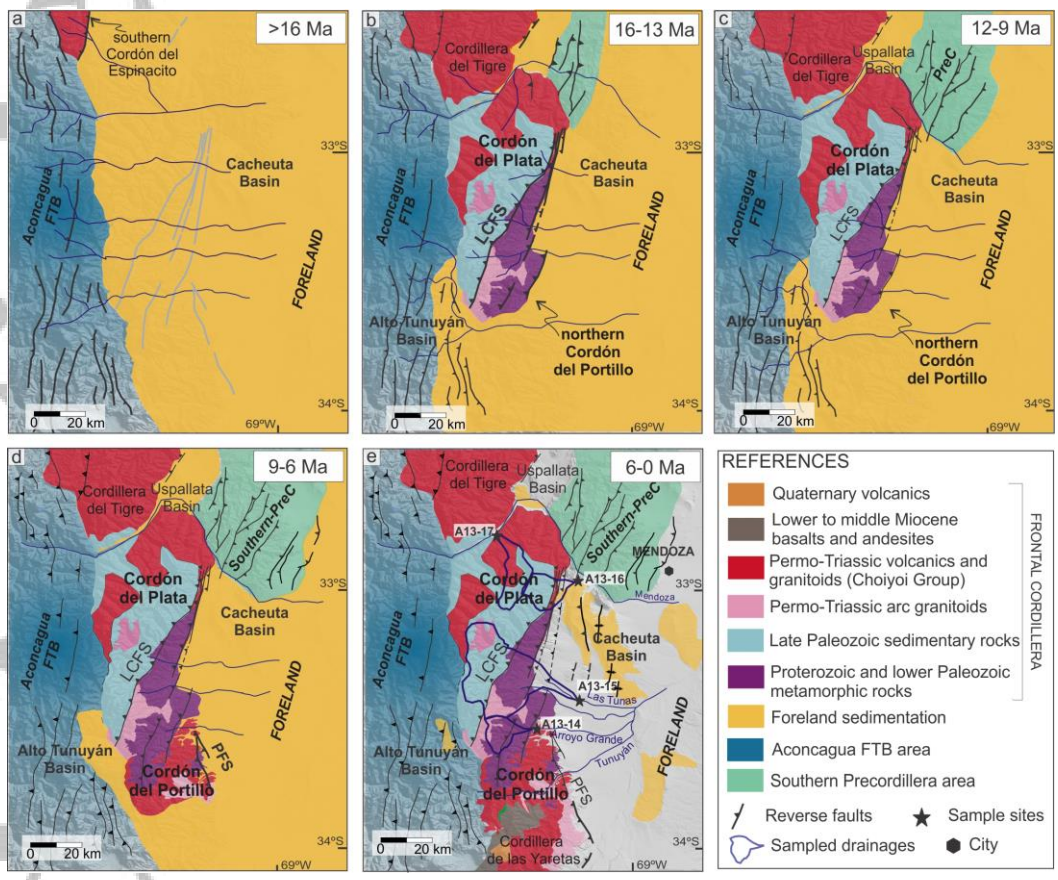

Figure 6: Timing of Miocene faulting in the Frontal Cordillera (Cordón del Plata and Cordón del Portillo) and syntectonic foreland sedimentation, based on the integration of thermochronology, geochronology, stratigraphic studies and field observations. (a) Previous to 16 Ma, deformation focused in the Aconcagua fold-and-thrust belt (AFTB) and the Cordón del Espinacito further north. Grey lines show Paleozoic inherited discontinuities reactivated during the Miocene. (b) At 16 Ma main rock uplift of Cordón del Plata and northern sector of Cordón del Portillo occurred with activity of La Carrera fault system and minor thrust activity in the Aconcagua FTB. By this time, the southern portion of Cordillera del Tigre and westernmost sector of Precordillera probably rose as suggested by provenance studies in the Cacheuta Basin (Buelow et al., 2018). (c) Remaining eastern sector of Precordillera rose (Buelow et al., 2018). (d) Between 9 to 6 Ma, deformation on the Portillo fault system and rock uplift of the southern Cordón del Portillo, as evidenced by provenance trends in Alto Tunuyán Basin (Palomares Formation). Overall, the locus of deformation shifted foreland-ward during lower Miocene to Present. LCFS: La Carrera fault system, PFS: Portillo fault system, PreC: Precordillera.

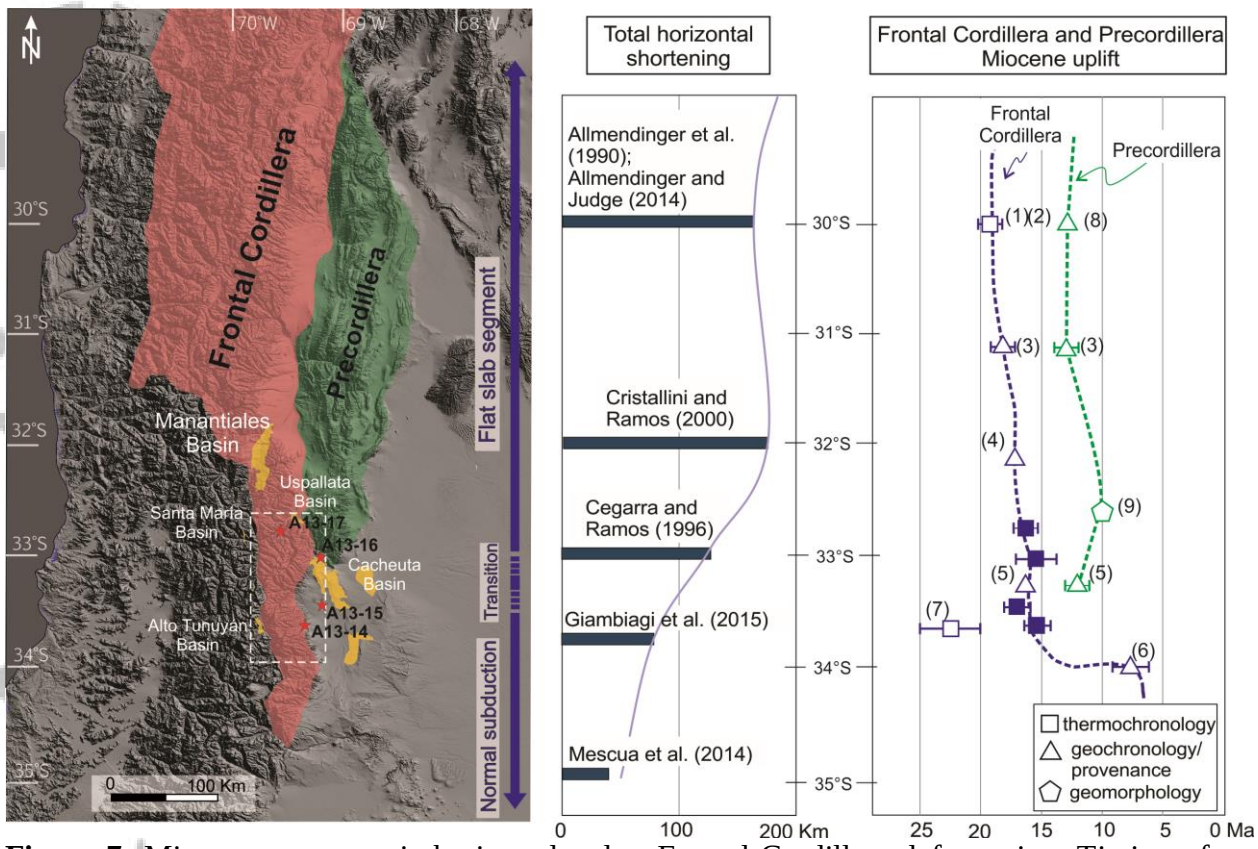

Figure 7: Miocene synorogenic basins related to Frontal Cordillera deformation. Timing of Miocene uplift and exhumation of the Frontal Cordillera and Precordillera, and total horizontal shortening based on available data. (1) Lossada et al. (2017), (2) Rodriguez et al. (2018), (3) Levina et al. (2014), (4) Mazzitelli et al. (2015), (5) Buelow et al. (2018), (6) Giambiagi et al. (2003), (7) Riesner et al. (2019), (8) Suriano et al. (2017), (9) Walcek and Hoke (2012).